Geometrically exact post-buckling and post-flutter of standing cantilevered pipe conveying fluid

Amir Mehdi Dehrouyeh-Semnani[1]

School of Mechanical Engineering, College of Engineering, University of Tehran, Tehran, Iran

Abstract

Although the nonlinear dynamics of hanging cantilevered pipe conveying fluid have been extensively scrutinized, a few investigations exist about the nonlinear behavior of standing one. Hence, the objective of this study is to examine the geometrically exact nonlinear static and dynamic responses of standing cantilevered pipe conveying fluid. The geometrically exact rotation-based model, along with the shooting method and Galerkin technique is applied to assess the nonlinear static behavior of system and its stability characteristics. Moreover, to compute the nonlinear dynamics of system, the geometrically exact quaternion-based model, together with the Galerkin technique is employed. It is revealed that the system may undergo buckling via a supercritical or subcritical pitchfork bifurcation depending on the gravity parameter, which may give rise to extremely large-amplitude responses. The system may also experience flutter instability via a supercritical Hopf bifurcation, which brings about self-excited periodic oscillations. The generic behavior of system for a specific range of the gravity parameter is investigated for four distinct scenarios depending on the gravity parameter and mass ratio, which only one of them is similar to that comes to pass for the hanging case.

Keywords

Standing cantilevered pipe conveying fluid; Geometrically exact nonlinear analysis; Subcritical and supercritical pitchfork bifurcation; Supercritical Hopf bifurcation; Extremely large amplitude; Self-excited periodic oscillation.

1. Introduction

Pipes conveying fluid as a kind of fluid-solid interaction system have drawn noteworthy research interest due to their applications in numerous engineering systems [1-6]. It is well-known that fluid-conveying pipes supported at both ends undergo buckling instability at a sufficiently high flow velocity [3, 7] and their nonlinear dynamic behavior has been widely analyzed [8-16]. According to the existing literature, the theoretical and experimental studies on the flutter instability of cantilevered pipes conveying fluid first appeared in the papers by Bourrières [17], Benjamin [18, 19], and Païdoussis and Gregory [20, 21]. Baja et al. [22, 23] developed a nonlinear mathematical model to study the bifurcation analysis of cantilevered pipe conveying fluid and some interesting features of system were reported in their studies. However, their nonlinear

[1] Email addresses: a.m.dehrouye@ut.ac.ir, a.m.dehrouye@gmail.com (A.M. Dehrouyeh-Semnani)

mathematical model has some incomplete terms which are discussed in detail in Ref. [3]. Semler et al. [24] established a third-order approximation nonlinear mathematical model for planner motion of cantilevered pipe conveying fluid, and Wadham-Gagnon et al. [25] developed it for three-dimensional motion. In many studies related to the cantilevered pipe conveying fluid, the third-order approximation model or its modified versions (due to added elements, imperfect support, material properties, and so on) have been utilized to study the nonlinear dynamics of system [26-35]. Since the third-order approximation model was derived [24] based on the inextensibility assumption, Ghayesh et al. [36] developed a new approximation model, which the third-order approximation model can be recovered from it, to investigate the role of extensibility in the nonlinear dynamics of cantilevered pipe conveying fluid.

Recently, the geometrically exact modeling and analysis of cantilevered pipe conveying fluid have drawn notable research interest due to the limitation of the third-order approximation model in the simulation of large-amplitude responses of system. The geometrically exact models for dynamic analysis have been developed based on four different approaches. In the first approach, a geometrically exact model based on the Cosserat rod model and applying balance laws for the linear and angular momentum using an intrinsic orthogonal framework [37]. In the second approach, a geometrically exact model based on the total moment of the fluid and pipe was proposed [38]. The fully nonlinear differential governing equations of system were established according to the momentum balance of pipe and fluid in floating non-inertial frames. The third approach is related to developing a geometrically exact model in terms of the rotation angle based on Hamilton's principle where the third-order approximation model can be recovered from this model [39-45]. The fourth approach is associated with the derivation of a geometrically exact model based on the quaternion formulation, along with Hamilton's principle [46]. It was indicated that the rotational-based model developed in Ref. [39] can be recovered from the newly developed model. A major difference between this model and that developed in Ref. [39] is that its governing equations are expressed in terms of integro-partial differential algebraic equations while the governing equation of the model presented in Ref. [39] is an integro-partial differential equation. The comparison studies indicated that the quaternion-based model is capable of capturing the nonlinear dynamics of system with a remarkable reduction in computational cost compared to the rotation-based model.

The nonlinear dynamics of standing cantilevered pipe conveying fluid have been investigated in a few studies. Li and Paidoussis [47] examined the nonlinear dynamics of standing cantilevered pipe conveying fluid via the third-order approximation model, together with the Galerkin technique with two modes. Prior to applying Galerkin's technique, the non-linear inertia terms were replaced by equivalent ones through a perturbation procedure. The focus of this study was on the stability and double degeneracy, where the subcritical pitchfork bifurcation and Hopf bifurcation take place simultaneously, as well as on the chaotic motion of system. Wang and Ni [48] studied the stability and chaotic motions of standing cantilevered pipe conveying fluid with elastic support and motion-limiting constraints. In the mathematical model, the source of

nonlinearity was the support and constraints, and a linear model was adopted for the pipe conveying fluid. Similar to the previous reference, Galerkin's technique with two modes was used to analyze the system. Bou-Rabee et al. [49] studied the stability characteristics of standing cantilevered pipe conveying fluid using a simple geometrically exact model. To construct the mathematical model, they supposed that the fluid-structure interaction induces a concentrated force and a point source of damping, respectively, tangent and normal to the free end. A long, thin conduit with a nozzle at its free end can be an appropriate representation for this model. Chen et al. [50] analyzed the nonlinear behavior of standing cantilevered pipe conveying fluid based on the geometrically exact rotation-based model for a specific case (see Appendix A).

The review of the papers related to the nonlinear analysis of cantilevered pipes conveying fluid shows that the nonlinear dynamics of standing system have not been disclosed appropriately, unlike the hanging and horizontal systems. Therefore, the focus of this paper is on exploring the geometrically exact nonlinear static and dynamic behavior of standing cantilevered pipe conveying fluid. In Section 2, two different mathematical models utilized to acquire the geometrically exact nonlinear responses of system are explained in detail. As well, the solution strategies for determining the static, stability, and dynamic behavior of system are elucidated. In Section 3, the available results in the existing literature related to the geometrically exact nonlinear dynamics of standing cantilevered pipe conveying fluid are employed to verify the mathematical model and solution strategy used in this paper for dynamic analysis. A convergence study on the verified results is also presented in this section. In Section 4, a geometrically exact nonlinear analysis of the generic behavior of system is carried out. Firstly, the stability of undeformed configuration of system without flow velocity due to gravity, along with its stable positions is studied. Subsequently, the influence of flow velocity, together with the gravity parameter on new static responses and their stability are examined. The role of flow velocity, along with the gravity parameter and mass ratio in the dynamic instability and corresponding motion characteristics is also investigated. A generic behavior for four distinct scenarios is discussed in detail. Additionally, the impact of initial conditions on the final response of system is explored. Eventually, the summary of findings is presented in Section 5.

2. On mathematical models and solution strategies

A schematic representation of a standing cantilevered pipe conveying fluid is depicted in Figure 1. The system under investigation includes a pipe of length L, cross-sectional area A, flexural rigidity EI, mass per unit length m, conveying a fluid of mass per unit length M with flow velocity $\overline{U}$.

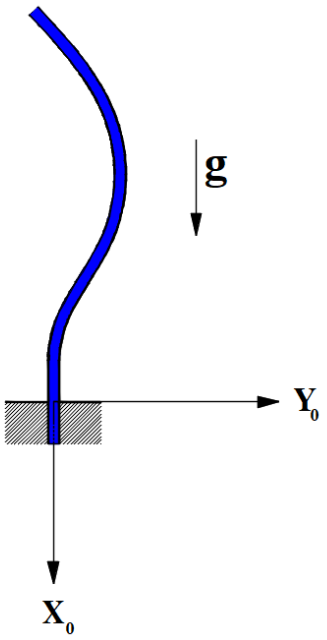

Figure 1: Schematic representation of a standing cantilevered pipe conveying fluid

To assess the geometrically exact static responses of system, the geometrically exact rotation-based model (GERM) is used. The reason for choosing this model is that it can easily capture the static responses of system in conjunction with the shooting scheme. However, their stability is determined by Galerkin's technique. The geometrically exact quaternion-based model (GEQM), along with the Galerkin technique is implemented for the dynamic analysis. The advantage of this model compared to the former model is its low computational cost. It should be pointed out that the mathematical models of hanging and standing cantilevered pipe conveying fluid are identical except for the gravity parameter. In the case of the hanging pipe, the gravity parameter is positive, but this parameter is negative for the standing pipe. Thus, the geometrically exact mathematical models of hanging cantilevered pipe conveying fluid developed in the previous studies can be utilized for the standing one. Static and stability analysis via GERM

2.1. Static and stability analyses via GERM

The dimensionless form of geometrically exact equation of motion and corresponding boundary conditions of cantilevered pipe conveying fluid in terms of rotation angle, θ, were established as follows [39, 40, 50]

$$\begin{aligned}
&\theta'' + (1-s)\gamma \sin(\theta) - \alpha\dot{\theta}'' + U^2 \sin(\theta(1) - \theta) \\
&+ \cos(\theta) \int_1^s \left[\int_0^{\hat{s}} \left((\dot{\theta})^2 \sin(\theta) - \ddot{\theta} \cos(\theta) \right) d\hat{s} \right] d\hat{s} \\
&- \sin(\theta) \int_1^s \left[\int_0^{\hat{s}} \left((\dot{\theta})^2 \cos(\theta) + \ddot{\theta} \sin(\theta) \right) d\hat{s} \right] d\hat{s} \\
&- 2U\sqrt{\beta} \left(\sin(\theta) \int_1^s \dot{\theta} \sin(\theta)\, d\hat{s} + \cos(\theta) \int_1^s \dot{\theta} \cos(\theta)\, d\hat{s} \right) = 0,
\end{aligned} \tag{1}$$

$$\theta(0) = 0, \ \theta'(1) = 0, \tag{2}$$

where the dimensionless parameters are

$$s = \frac{s^*}{L}, \ (\tau, \alpha) = \sqrt{\frac{EI}{(M+m)L^4}} (t, \alpha^*), \ \mathrm{U} = \left(\frac{M}{EI} \right)^{1/2} \bar{\mathrm{U}}, \ \beta = \frac{M}{M+m}, \ \gamma = \frac{M+m}{EI} gL^3, \tag{3}$$

in which s is dimensionless distance along the pipe from the clamped end, ζ and η, respectively, are dimensionless axial and transverse displacements, τ is dimensionless time, α is dimensionless damping coefficient, U is dimensionless flow velocity, β is mass parameter, and γ is gravity parameter. Moreover, the prime and dot symbols denote derivatives with respect to s and τ, respectively. The dimensionless axial and transverse displacements, respectively, can be obtained by [39]

$$\zeta = \frac{u}{L} = \int_0^s \cos(\theta(\hat{s}))\, d\hat{s} - 1, \ \eta = \frac{v}{L} = \int_0^s \sin(\theta(\hat{s}))\, d\hat{s}. \tag{4}$$

The geometrically exact rotation-based static model can be achieved by dropping the time-dependent terms in Eq. (1) [50].

$$\theta_s'' + (1-s)\gamma \sin(\theta_s) + U^2 \sin(\theta_s(1) - \theta_s) = 0, \tag{5}$$

in which θ_s stands for static rotation angle. Similar to Ref. [51], the shooting scheme is used to evaluate the geometrically exact responses of system based on the static equation given in Eq. (5). To determine their stability, the linearized dynamic model around the static responses is employed. Substituting $\theta + \theta_s$ instead of θ in Eq. (1), incorporating Eq. (5), and neglecting nonlinear terms in the resulting equation, one can obtain the following linear dynamic equation [50].

$$\begin{aligned}
&\theta'' + (1-s)\gamma \sin(\theta^s)\theta - \alpha\dot{\theta}'' + U^2 (\theta(1) - \theta) \cos(\theta^s(1) - \theta^s) \\
&+ \cos(\theta^s) \int_1^s \left[\int_0^{\hat{s}} -\ddot{\theta} \cos(\theta^s)\, ds' \right] d\bar{s} - \sin(\theta^s) \int_1^s \left[\int_0^{\hat{s}} \ddot{\theta} \sin(\theta^s)\, d\hat{s} \right] d\hat{s} \\
&- 2U\sqrt{\beta} \left(\sin(\theta^s) \int_1^s \dot{\theta} \sin(\theta^s)\, d\hat{s} + \cos(\theta^s) \int_1^s \dot{\theta} \cos(\theta^s)\, d\hat{s} \right) = 0,
\end{aligned} \tag{6}$$

In view of Galerkin's technique, the rotation angle is approximated as follows

$$\theta = \sum_{n=1}^{N} \varphi_n p_n, \tag{7}$$

in which N, φ_n and p_n stand for number of approximation functions, nth approximation function, and nth generalized coordinate, respectively. Similar to Ref. [50], $\varphi_n = sin((2n-1)\pi s/2)$. It should be mentioned that to calculate the stability characteristics of system around its undeformed configuration, it is enough to set $\theta_s = 0$ in Eq. (6).

2.2. Dynamic analysis via GEQM

The geometrically exact mathematical model of cantilevered pipe conveying fluid in the quaternion system was derived in Ref. [46]. The quaternion elements e_0 and e_3 can be written in terms of the rotation angle as follows [46]: $e_0 = cos(\theta/2)$ and $e_3 = sin(\theta/2)$, along with the following constraint: $\Phi = e_0^2 + e_3^2 = 1$. The resulting dimensionless form of this mathematical model is [46]

$$
\begin{aligned}
&4\left(e_0''e_3^2 - e_0e_3e_3'' - 2e_0\left(e_3'\right)^2 + 2e_0'e_3e_3'\right) + \gamma\left(2e_0\right)\left(1-s\right)\\
&+\left[2e_0\int_1^s\int_0^{\hat{s}} 2\left(e_0\ddot{e}_0 + \left(\dot{e}_0\right)^2 - e_3\ddot{e}_3 - \left(\dot{e}_3\right)^2\right)d\bar{s}d\hat{s}\right] + \left[2e_3\int_1^s\int_0^{\hat{s}} 2\left(e_0\ddot{e}_3 + 2\dot{e}_0\dot{e}_3 + e_3\ddot{e}_0\right)d\bar{s}d\hat{s}\right]\\
&+2U\sqrt{\beta}\left(\left[2e_0\int_1^s 2\left(e_0\dot{e}_0 - e_3\dot{e}_3\right)d\hat{s}\right] + \left[2e_3\int_1^s 2\left(e_3\dot{e}_0 + \dot{e}_3e_0\right)d\hat{s}\right]\right)\\
&-U^2\left[2e_0\left(e_0^2(1) - e_3^2(1)\right) + 2e_3\left(2e_0(1)e_3(1)\right)\right] - \alpha\left[-8\left(e_3'e_3\dot{e}_0' + e_3'e_0'\dot{e}_3 - e_3'e_3'\dot{e}_0 - e_3'e_0\dot{e}_3'\right) -\right.\\
&\left.4\left(e_3e_3'\dot{e}_0' + e_3e_3\dot{e}_0'' + e_3e_0'\dot{e}_3' + e_3e_0''\dot{e}_3 - e_3e_3''\dot{e}_0 - e_3e_3'\dot{e}_0' - e_3e_0\dot{e}_3'' - e_3e_0'\dot{e}_3'\right)\right] - 2e_0\lambda = 0,
\end{aligned}
\tag{8}
$$

$$
\begin{aligned}
&4\left(e_0^2e_3'' - e_0e_0''e_3 - 2\left(e_0'\right)^2e_3 + 2e_0e_0'e_3'\right) - \gamma\left(2e_3\right)\left(1-s\right)\\
&-\left[2e_3\int_1^s\int_0^{\hat{s}} 2\left(e_0\ddot{e}_0 + \left(\dot{e}_0\right)^2 - e_3\ddot{e}_3 - \left(\dot{e}_3\right)^2\right)d\bar{s}d\hat{s}\right] + \left[2e_0\int_1^s\int_0^{\hat{s}} 2\left(e_0\ddot{e}_3 + 2\dot{e}_0\dot{e}_3 + e_3\ddot{e}_0\right)d\bar{s}d\hat{s}\right]\\
&-2U\sqrt{\beta}\left(\left[2e_3\int_1^s 2\left(e_0\dot{e}_0 - e_3\dot{e}_3\right)d\hat{s}\right] - \left[2e_0\int_1^s 2\left(e_3\dot{e}_0 + \dot{e}_3e_0\right)d\hat{s}\right]\right)\\
&-U^2\left[-2e_3\left(e_0^2(1) - e_3^2(1)\right) + 2e_0\left(2e_0(1)e_3(1)\right)\right] - \alpha\left[8\left(e_0'e_3\dot{e}_0' + e_0'e_0'\dot{e}_3 - e_0'e_3'\dot{e}_0 - e_0'e_0\dot{e}_3'\right) +\right.\\
&\left.4\left(e_0e_3'\dot{e}_0' + e_0e_3\dot{e}_0'' + e_0e_0'\dot{e}_3' + e_0e_0''\dot{e}_3 - e_0e_3''\dot{e}_3 - e_0e_3'\dot{e}_0' - e_0e_0\dot{e}_3'' - e_0e_0'\dot{e}_3'\right)\right] - 2\lambda e_3 = 0,
\end{aligned}
\tag{9}
$$

$$
e_0^2 + e_0^3 = 1, \tag{10}
$$

$$
e_0(0) = 1,\ e_3(0) = 0,\ e_0'(1) = 0,\ e_3'(1) = 0, \tag{11}
$$

in which λ is dimensionless Lagrangian multiplier function. The dimensionless axial and transverse displacements in terms of the quaternion elements, respectively, can be written [46]

$$
\zeta = \int_0^s\left(e_0^2 - e_3^2\right)d\hat{s} - 1,\ \ \eta = \int_0^s 2e_0e_3\ d\hat{s}. \tag{12}
$$

The mathematical model of system in terms of the rotation angle is an integro-partial differential equation (Eqs. (1)-(2)), but it is an integro-partial differential algebraic equation in terms of the quaternion elements (Eqs. (8)-(11)). In Ref. [46], it was proved that Eqs. (1)-(2) can be recovered

from Eqs. (8)-(11). Furthermore, it was discussed that the quaternion-based model significantly reduces the computational cost compared to the rotation-based model.

In view of Galerkin's technique, the quaternion elements and the dimensionless Lagrangian multiplier function are approximated as follows

$$e_0 = 1 + \sum_{n=1}^{N_{e_0}} \phi_n p_n,\ e_3 = \sum_{n=1}^{N_{e_3}} \psi_n q_n,\ \lambda = \sum_{n=1}^{N_\lambda} \chi_n r_n \tag{13}$$

where N_{e_0}, N_{e_3}, and N_λ are number of approximation functions for e_0, e_3, and λ, respectively; ϕ_n, ψ_n, and χ_n are nth approximation function for e_0, e_3, and λ, respectively; p_n, q_n, and r_n are nth generalized coordinate of e_0, e_3, and λ, respectively. Similar to Ref. [46], $N_{e_0} = N_{e_3} = N_\lambda = N$, $\phi_n = \psi_n = sin((2n-1)\pi s/2)$ and $\chi_n = sin(n\pi\,(s+0.5)/4)$.

Similar to Ref. [46], to solve the resulting ordinary differential algebraic equations, the ode15s solver in MATLAB software is utilized. To reduce the index of resulting equations from three to one, Eq. (10) is replaced with the following equation [46]

$$\dot{e}_0^2 + \dot{e}_3^2 + e_0\ddot{e}_0 + e_3\ddot{e}_3 = 0. \tag{14}$$

which is the second derivative of Eq. (10) with respect to τ.

3. Verification study

In Ref. [46], the quaternion-based model was utilized to verify the geometrically exact nonlinear behavior of hanging cantilevered pipe conveying fluid. Therefore, in this section, this model is verified for the standing one. Chen et al. [50] investigated the nonlinear responses of a standing pipe conveying fluid when $\beta = 0.142$, $\gamma = -18.9$, and $\alpha = 0.005$ via the geometrically exact rotation-based model with $N = 4$. To verify the results reported by the aforementioned reference, the geometrically exact nonlinear responses of quaternion-based model with $N = 4$ and 5 are calculated. Comparison studies are presented in Appendix A. The comparison studies in Figures A1-A3 show that the results of quaternion-based model with $N = 4$ are in good agreement with those obtained by Chen et al. [50] via the rotation-based model. Additionally, the plots depicted in these figures indicate that the results with $N = 5$ can better describe the geometrically exact nonlinear dynamics of system.

4. Nonlinear geometrically exact analysis

For a hanging pipe with $U = 0$, the undeformed configuration of system is stable. But for a corresponding standing one, the stability of undeformed configuration is dependent on the gravity parameter. The geometrically exact nonlinear static responses and their stability characteristics for standing pipes when $-100 \le \gamma \le 0$ are plotted in Figure 2. The plots show that the undeformed configuration of system is stable if the gravity parameter is large enough. However, the undeformed configuration of system becomes unstable and the system undergoes buckling instability at a critical gravity parameter $\gamma^{cr} = -7.83$. In other words, the system buckles due to

its weight (self-buckling). The plots indicate that the system undergoes extremely large deformation when the gravity parameter is low enough. It should be stressed that the simple model proposed by Bou-Rabee et al. [49] is capable of capturing the geometrically exact static behavior of system. It is due to the fact that simplifying in their model does not affect the static instability of system. The results plotted in Figure 2a were presented in their work for $-60 \leq \gamma \leq 0$ based on a dynamic analysis. There is a good agreement between the present results and those reported in the aforementioned references.

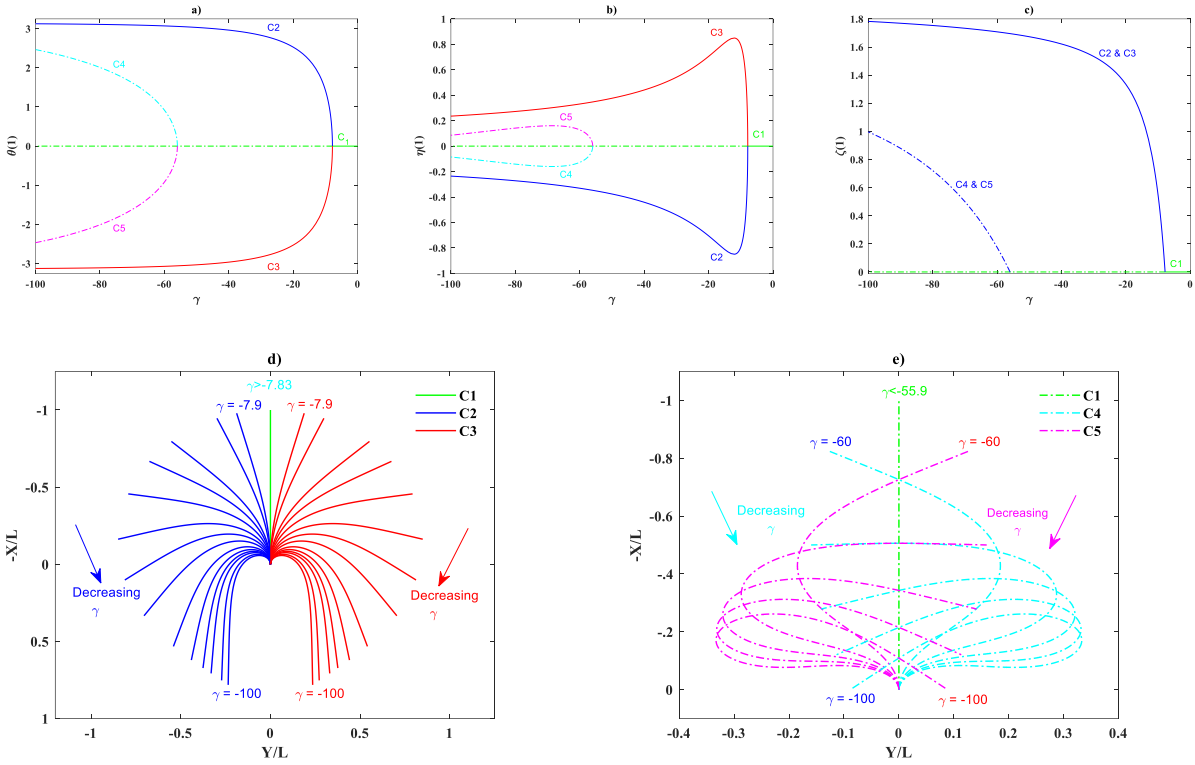

Figure 2: Evolution of the pipe shapes when $U = 0$; a) tip rotation, b) tip transverse displacement, c) tip axial displacement, d) stable shapes, e) unstable shapes.

The influence of flow velocity, U, on the static instability of system is depicted in Figure 3. The results illustrate that the system experiences supercritical pitchfork bifurcation (buckling) when $-14 \leq \gamma < -7.83$. In other words, for this range of gravity parameter, the undeformed configuration of system becomes stable at a critical flow velocity, U_{super}. Besides, U_{super} is increased when the gravity parameter is decreased. The results also indicate that the system undergoes a subcritical pitchfork bifurcation (buckling) when $\gamma < -14$. The lower subcritical velocity,U_{sub}^{low}, has an initial ascending trend which follows by a descending one when the gravity parameter is reduced. Since U_{sub}^{low} becomes zero for $\gamma = -55.9$, the lower subcritical velocity does not exist for the system when $\gamma < -55.9$. Additionally, the higher subcritical velocity, U_{sub}^{high}, has an ascending trend with respect to lessening the gravity parameter. It should be pointed out that the supercritical critical flow velocities in addition to the lower subcritical flow velocities can be

obtained by the stability analysis of linear model around the undeformed configuration i.e., Eq. (6) when $\theta_s = 0$. The results of the present study are in good agreement with those reported by Paidoussis [3, 52] based on the linear analysis.

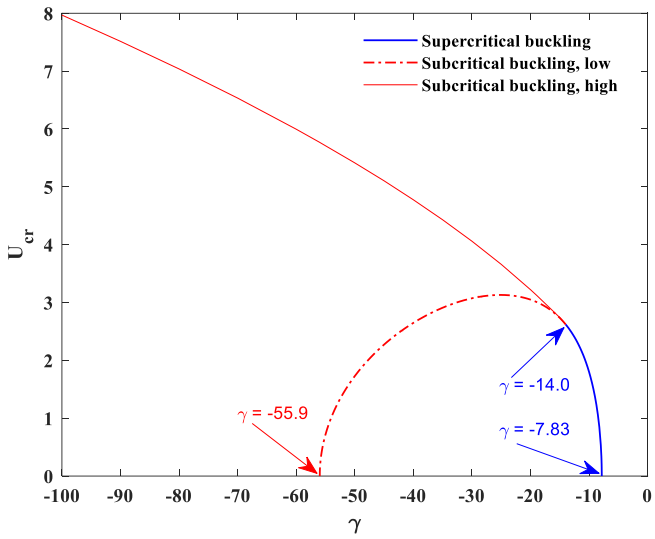

Figure 3: Locus of the critical flow velocities for the supercritical and subcritical buckling.

The geometrically exact post-buckling behavior of standing pipes conveying fluid are shown in Figures 4-6 for the tip rotation angle, axial and transverse displacements, respectively. Figures 4a, 5a, and 6a are related to the non-trivial post-supercritical buckling responses of system. As seen from the results plotted in these figures, when the flow velocity, U, is increased, the system undergoes less deformation, and at a critical flow velocity, U_{super}, the undeformed configuration of system becomes its stable position. It should be pointed out that for supercritical buckling, the undeformed configuration (the trivial solution) is unstable when $U < U_{super}$, but the stability behavior of system for $U > U_{super}$ is dependent on the mass parameter, β, and the damping coefficient, α. The other plots in Figures 4-6 are associated with the non-trivial post-subcritical buckling responses of system. Similar to supercritical buckling, the system experiences less deformation when the flow velocity is increased, but the trend stops at a critical flow velocity, U_{sub}^{high}, in which the system is under deformation. The results indicate that the difference in the deformation of system between $U = 0$ and U_{sub}^{high} diminishes when the gravity parameter, γ, is lessened. It should be stressed that the undeformed configuration of system (the trivial solution) is unstable when $U \leq U_{sub}^{low}$ and the stability of the trivial solution for $U > U_{sub}^{low}$ relies on β and α. It can be concluded when $U_{sub}^{high} \leq U < U_{sub}^{low}$, the undeformed configuration of system may be stable and the system has three distinct stable positions.

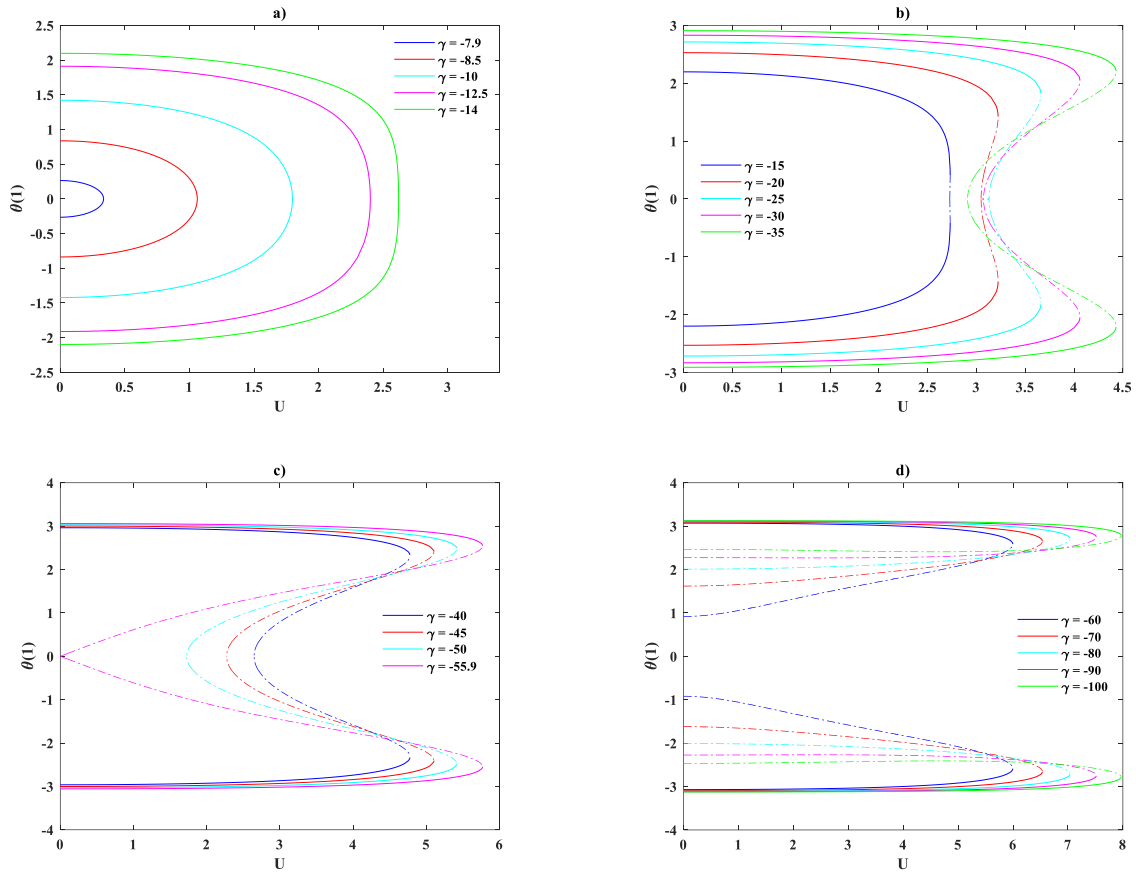

Figure 4: Stable (solid line) and unstable (dash-dot line) non-trivial solutions for the tip rotation of pipe in the post-buckling region.

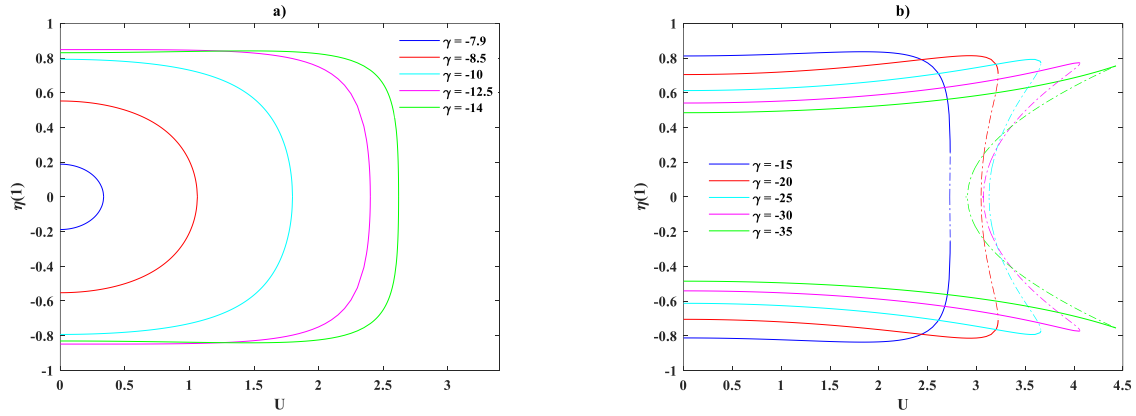

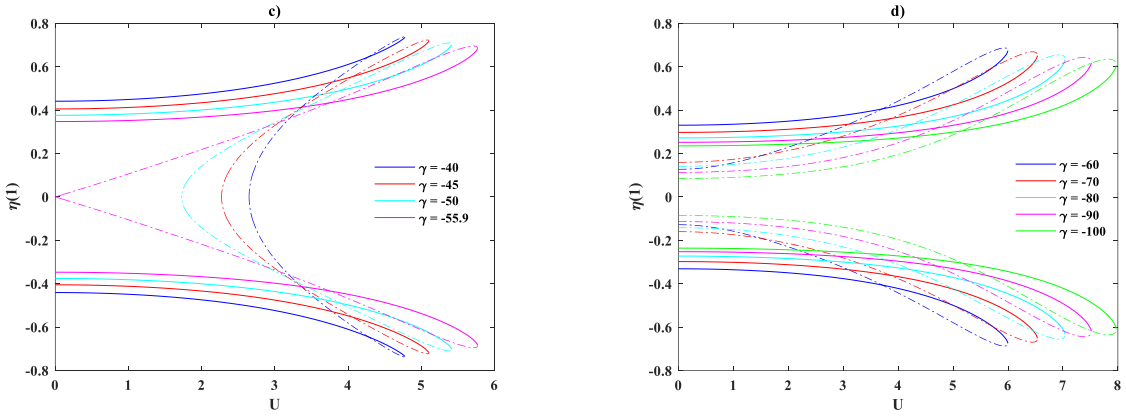

Figure 5: Stable (solid line) and unstable (dash-dot line) non-trivial solutions for the tip transverse displacement of pipe in the post-buckling region corresponding to Figure 4.

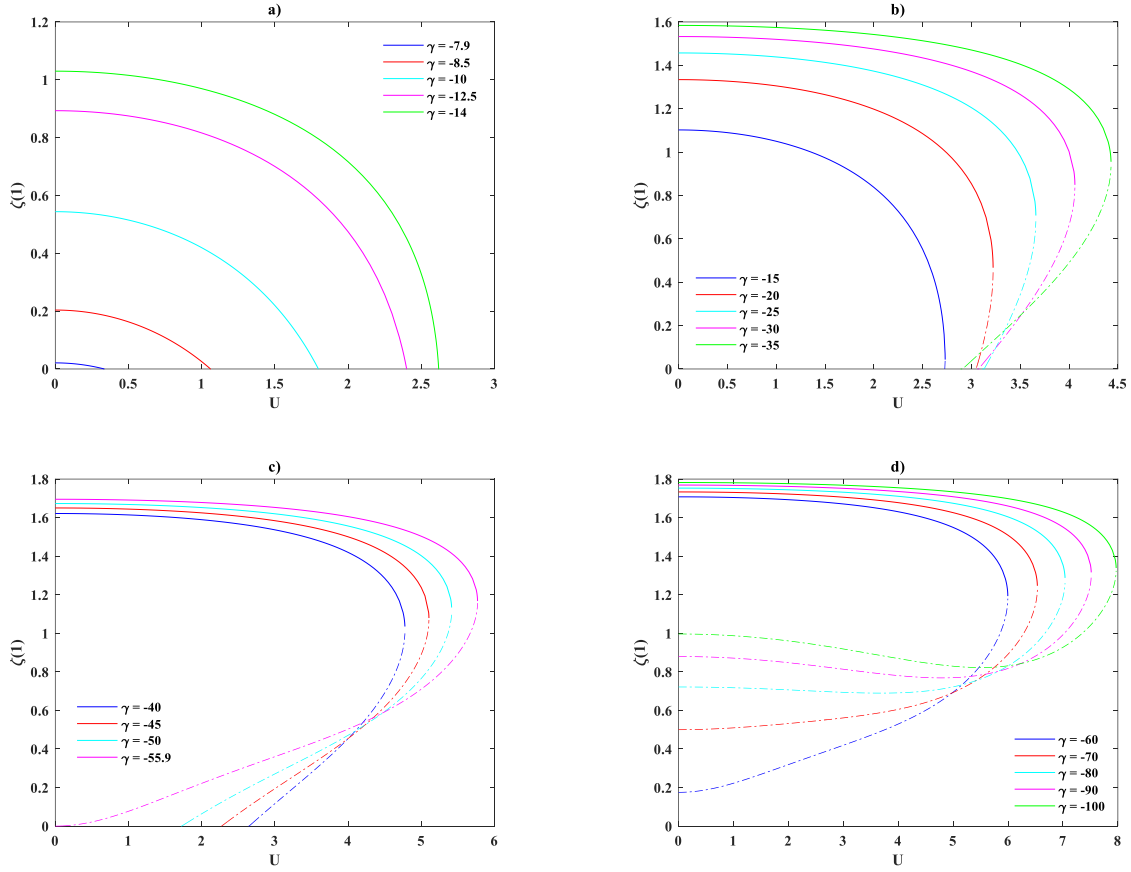

Figure 6: Stable (solid line) and unstable (dash-dot line) non-trivial solutions for the tip axial displacement of pipe in the post-buckling region corresponding to Figure 4.

Prior to starting dynamic analysis, it should be pointed out that in all the dynamic assessments, the damping coefficient, α, is set to 0.005 similar to Ref. [50]. Additionally, the whole dynamic responses are obtained with $N = 5$ in the Galerkin technique.

In the case of the hanging cantilevered pipe conveying fluid, the undeformed configuration of system is stable and becomes unstable at a critical flow velocity by a flutter instability i.e., the system experiences a supercritical Hopf bifurcation. As seen in Figure 7, a similar scenario occurs for the standing cantilevered pipe conveying fluid when the gravity parameter is large enough i.e., $\gamma < -7.83$. In the case of the supercritical buckling i.e., $-14 \leq \gamma < -7.83$, the system restabilizes at U_{super} and at a critical flow velocity, U^f, which depends the mass ratio, β, the system losses its stability via a flutter instability i.e., the system undergoes a supercritical Hopf bifurcation. In other words, for $-14 \leq \gamma < -7.83$, the undeformed configuration of system is stable when $U_{super} < U < U^f$. In the case of subcritical buckling i.e., $\gamma < -14$, different scenarios may take place depending on the gravity parameter and the mass ratio. For example, when $\gamma = -20$, the undeformed configuration of system becomes stable at $U_{sub}^{unstable}$ and it remains stable until U^f. Since $U^f > U_{sub}^{high}$, the undeformed configuration of system is stable for $U_{sub}^{low} < U \leq U_{sub}^{high}$ and the system has three different stable positions in the aforementioned range. For another example, when $\gamma = -30$ and $\beta = 0.17$ or 0.25, $U^f < U_{sub}^{high}$ which means the system has three different stable positions for $U_{sub}^{low} < U < U^f$ and the system undergoes post-supercritical buckling or post-flutter for $U^f < U < U_{sub}^{high}$. For $\gamma = -30$ and $\beta = 0.37$ or 0.45, the system experiences a similar scenario to $\gamma = -20$.

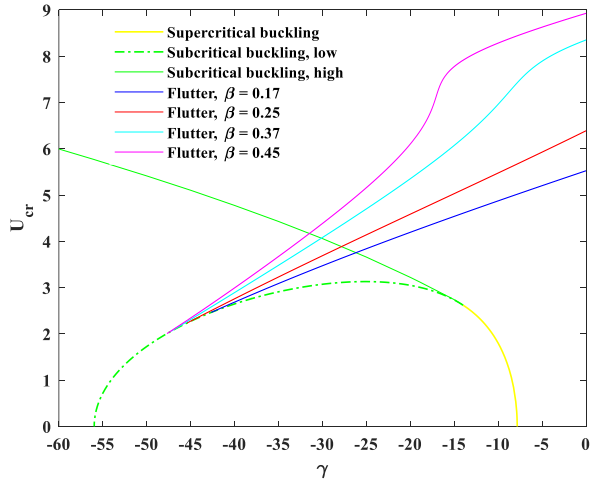

Figure 7: Locus of the critical flow velocities for the buckling and flutter instabilities.

The generic behavior of system with $\beta = 0.17$, $\gamma = -5$, -10, -20, and $0 \leq U \leq 10$ are displayed in Figures 8-10. As seen from the plots in these figures, the system undergoes three different scenarios depending on the gravity parameter, γ. In the first scenario related to $\gamma = -5$, the undeformed configuration of system is stable and then becomes unstable by a flutter instability at a critical flow velocity $U^f = 5.2006$. For the flow velocities greater than the critical one, the system experiences a supercritical Hopf bifurcation. In the second scenario corresponding to $\gamma = -10$, the undeformed configuration of system is unstable and the system has two symmetric stable positions related to the supercritical buckling. At a critical flow velocity $U_{super} = 1.7969$, two

stable positions vanish and the undeformed configuration of system becomes stable. Afterward, the undeformed configuration of system loses its stability at a critical flow velocity $U^f = 4.8732$ in which the system undergoes flutter instability by a supercritical Hopf bifurcation. In the third scenario associated with $\gamma = -20$, the system has two symmetric stable positions due to subcritical buckling when $U < U_{sub}^{high} = 3.2220$. The undeformed configuration of system is unstable until $U \leq U_{sub}^{low} = 3.0474$ and then becomes stable; therefore, the system finds three stable positions, along with two symmetric unstable positions when $3.0474 < U < 3.2220$. Afterwards, both the symmetric stable and unstable positions disappear and the undeformed configuration becomes unstable again due to the occurrence of supercritical Hopf bifurcation at $U^f = 4.1952$. It is worth noting that the plots in Figure 8 indicate the tip rotation angle of system rises when the flow velocity is increased for all three cases.

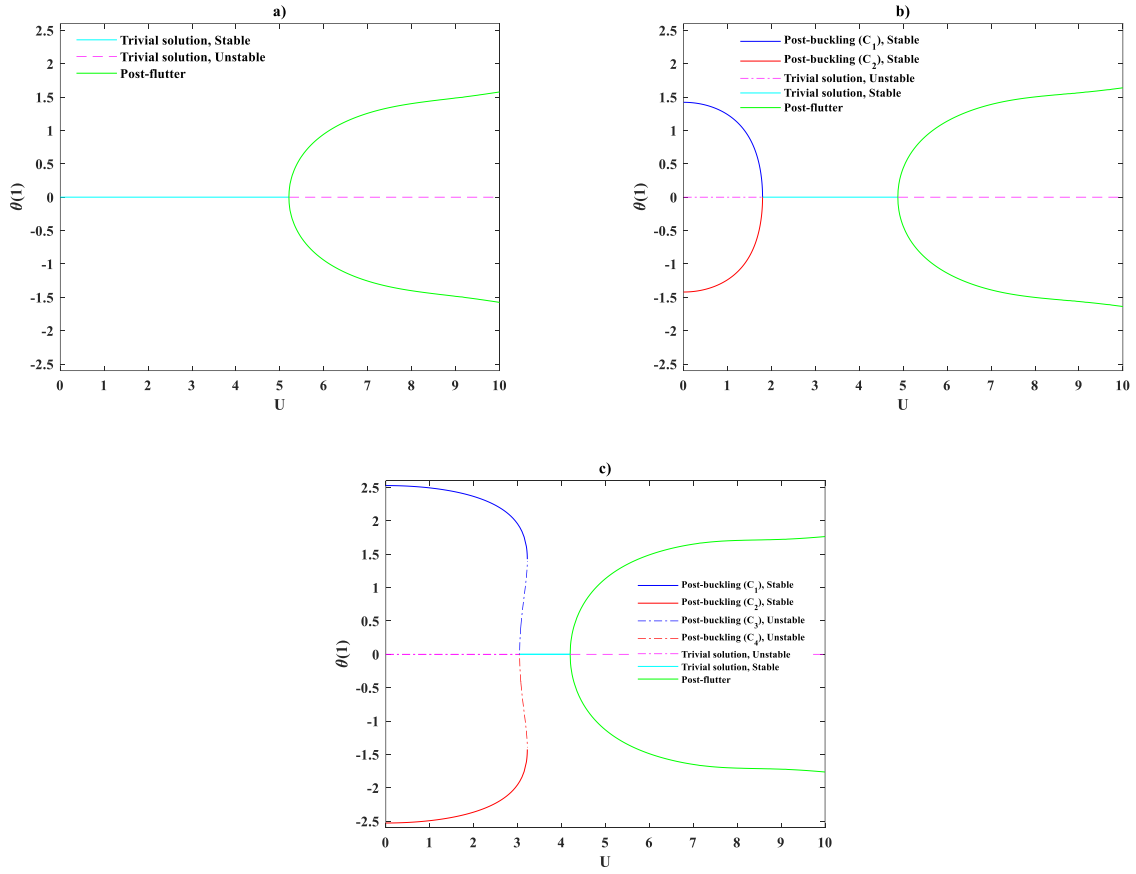

Figure 8: The tip rotation of pipe when $\beta = 0.17$; a) $\gamma = -5$, b) $\gamma = -10$, c) $\gamma = -20$.

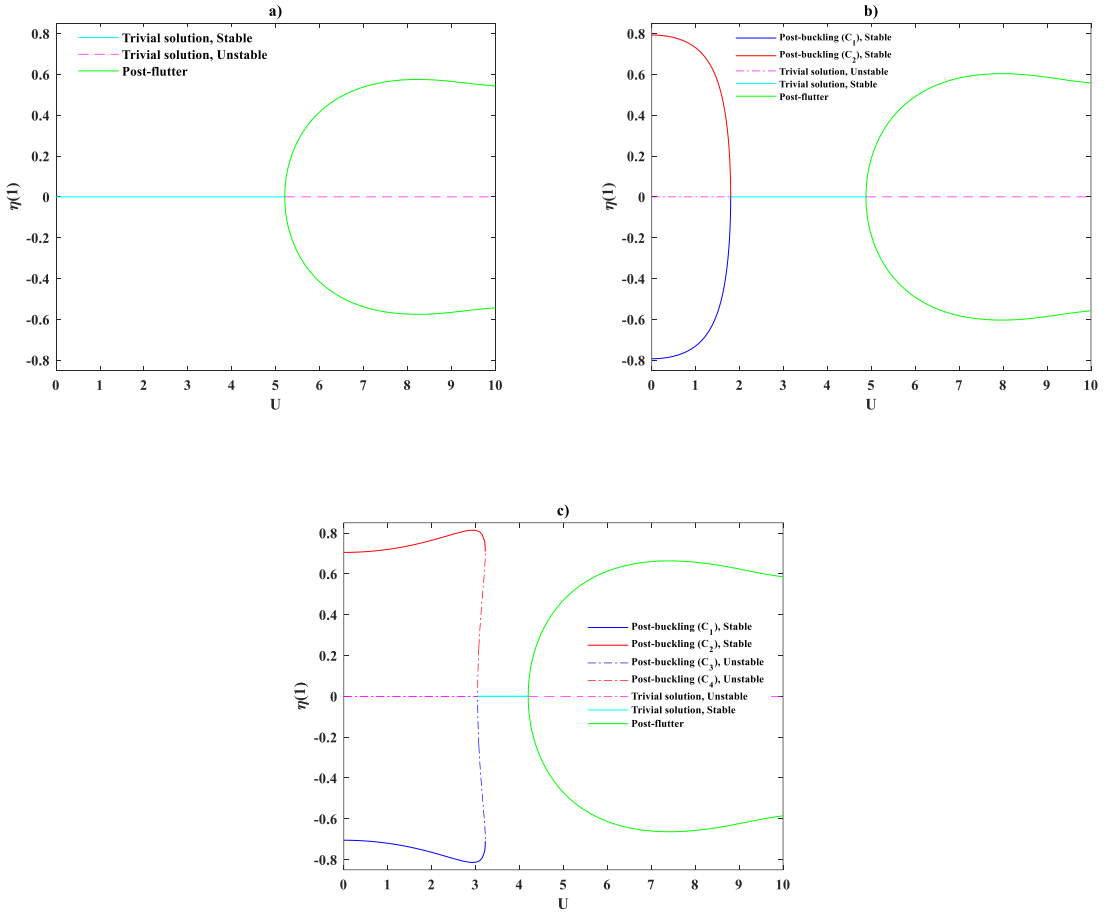

Figure 9: The tip transverse displacement of pipe corresponding to Figure 8; a) $\gamma = -5$, b) $\gamma = -10$; c) $\gamma = -20$.

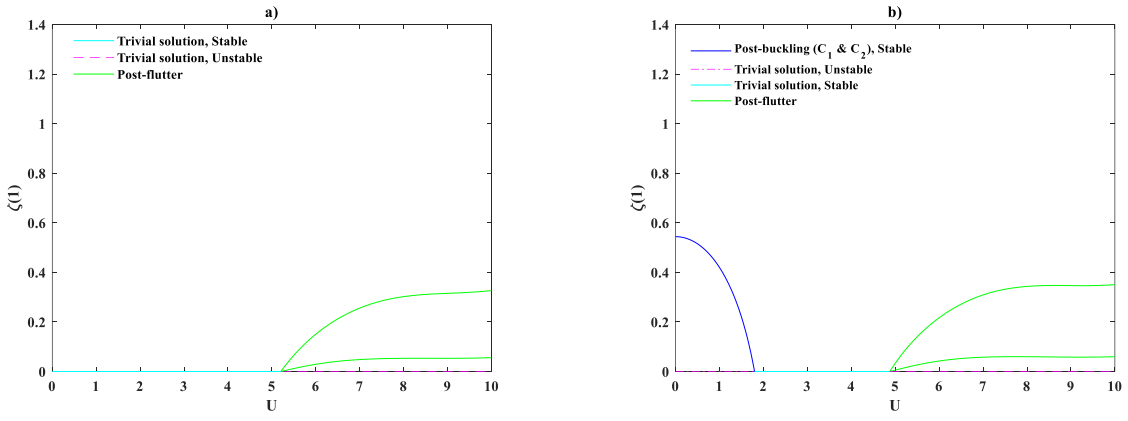

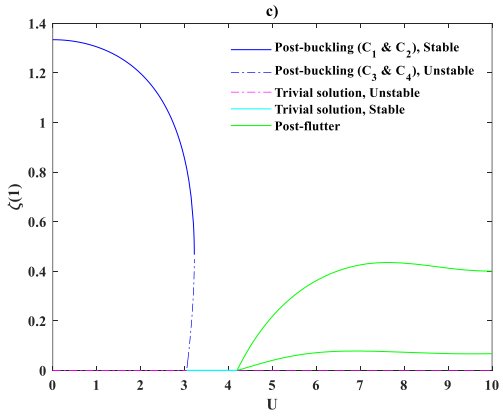

Figure 10: The tip axial displacement of pipe corresponding to Figure 8; a) $\gamma = -5$, b) $\gamma = -10$; c) $\gamma = -20$.

The two symmetric stable positions of system with $\gamma = -10$ and -20, respectively, pertinent to the supercritical and subcritical bucklings are shown in Figure 11. It can be observed when the flow velocity gradually rises, the system with $\gamma = -10$ settles down at its undeformed configuration for $U = 1.7969$. In the case of $\gamma = -20$, a different scenario exists due to a gradual increase in the flow velocity. The system is under deformation until $U = 3.2220$, but a small increase in this critical flow velocity results in a jump, and the system settles down at its undeformed configuration (see Figure 8c).

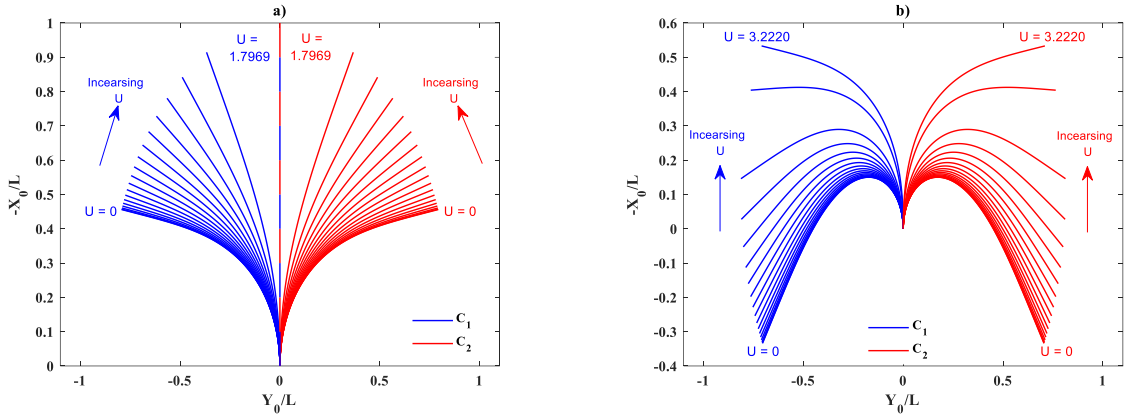

Figure 11: Evolution of the stable buckled shapes of pipe corresponding to the non-trivial solutions when $\beta = 0.17$; a) $\gamma = -10$ (supercritical buckling), b) $\gamma = -20$ (subcritical buckling).

The evolution of pipe shapes in the post-flutter region for the third case investigated in Figures 8-10 is exhibited in Figure 12. Additionally, the corresponding phase planes of system for the tip rotation angle, tip axial, and transverse displacements are displayed in Figure 13.

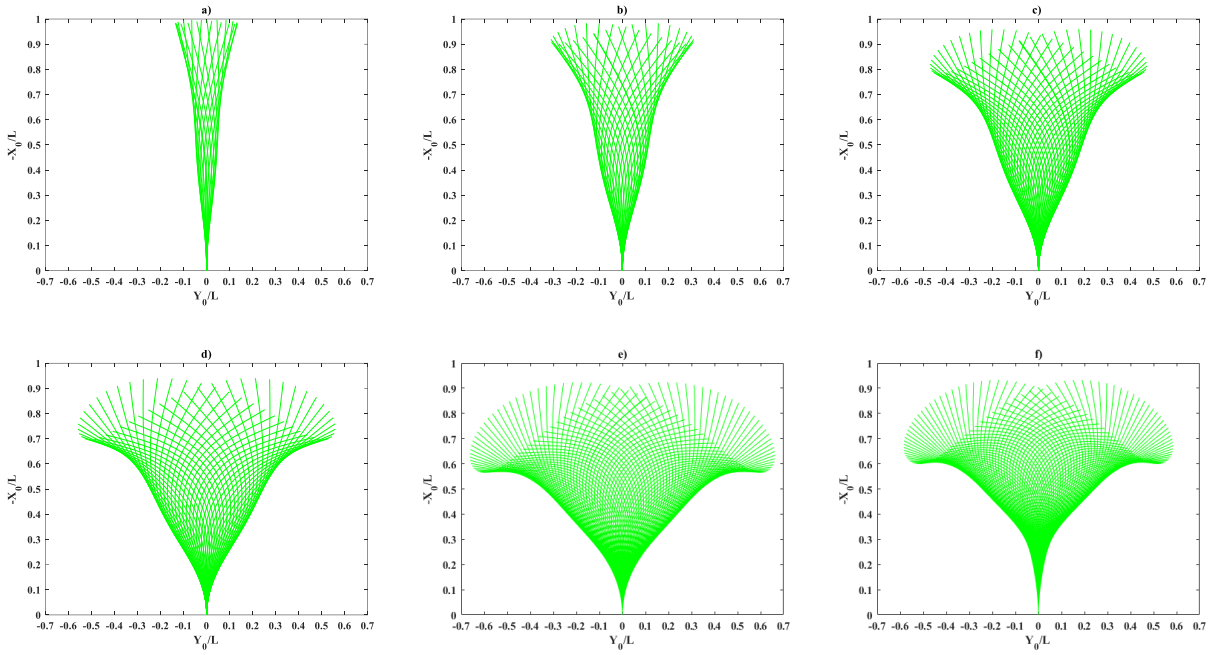

Figure 12: Shapes of the oscillating pipe in the post-flutter region when $\beta = 0.17$, $\gamma = -20$; a) $U = 4.25$, b) $U = 4.5$, c) $U = 5$, d) $U = 5.5$, e) $U = 7.5$, f) $U = 10$.

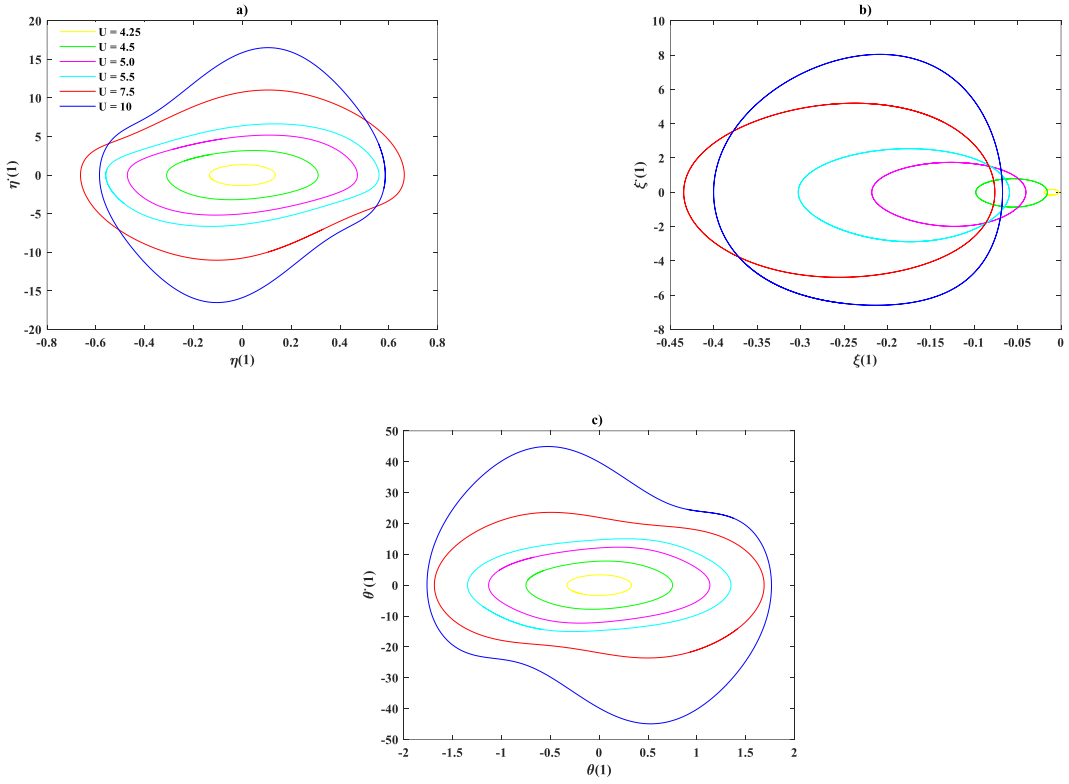

Figure 13: Phase planes of the oscillating pipe in the post-flutter region corresponding to Figure 12.

In view of Figure 7, the scenarios plotted for the system with $\beta = 0.17$ in Figures 8-10 can be similarly plotted for the systems with $\beta = 0.25, 37$, and 0.45 with an exception for the critical flow velocity associated with the flutter instability. Therefore, for the aforementioned cases, only their post-flutter responses are studied in Figures 14-17. In order to better compare the results, the post-flutter behavior of system with $\beta = 0.17$ are also shown in these figures.

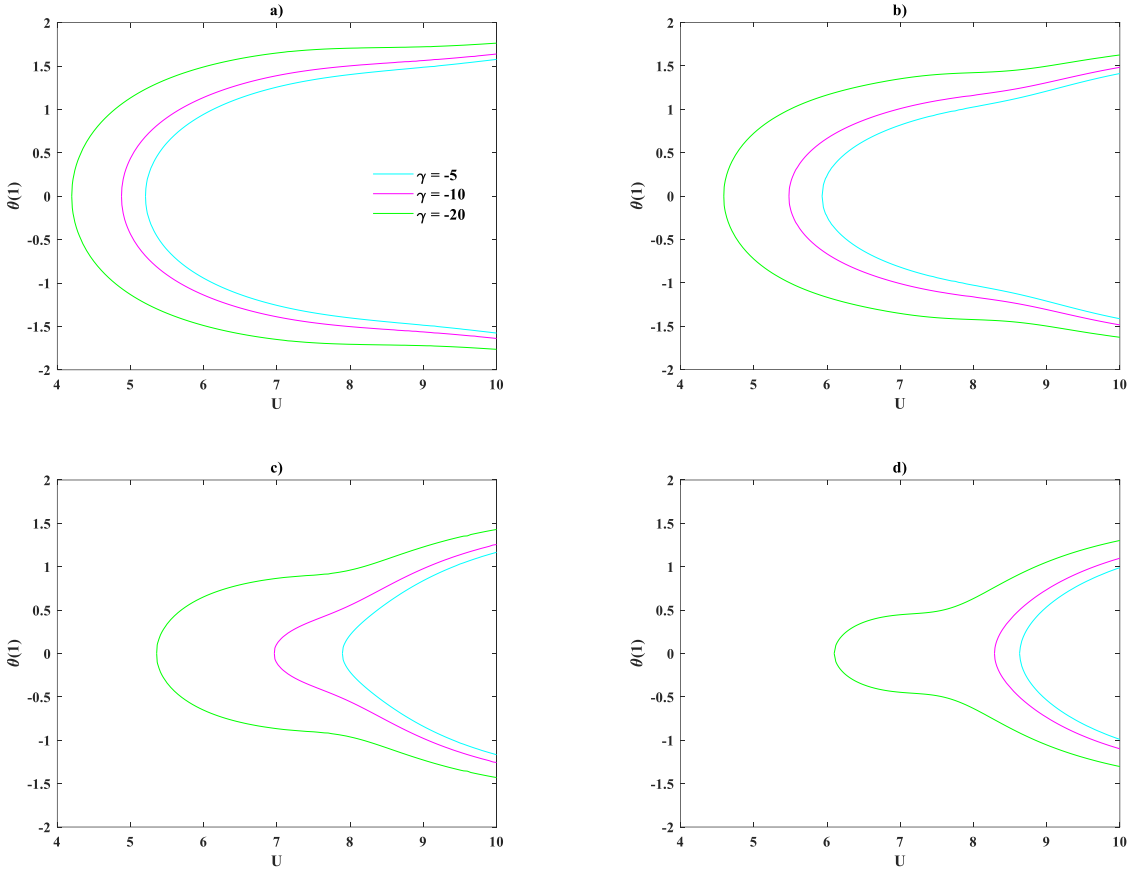

Figure 14: The tip rotation of pipe in the post-flutter region; a) $\beta = 0.17$, b) $\beta = 0.25$, c) a) $\beta = 0.37$, d) $\beta = 0.45$.

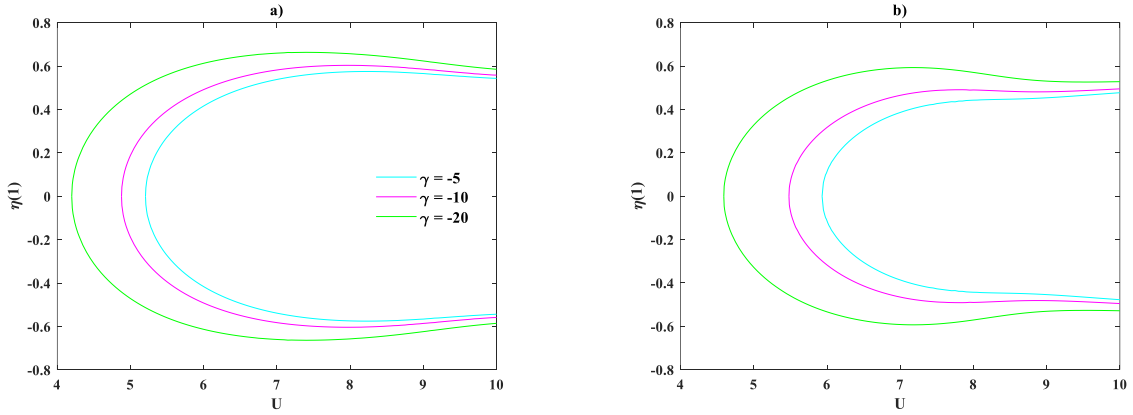

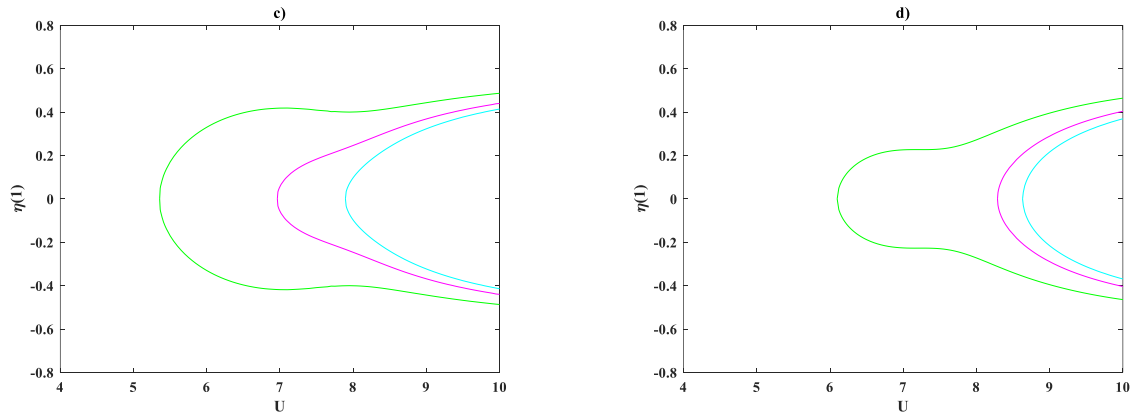

Figure 15: The tip transverse displacement of pipe in the post-flutter region corresponding to Figure 14; a) $\beta = 0.17$, b) $\beta = 0.25$, c) a) $\beta = 0.37$, d) $\beta = 0.45$.

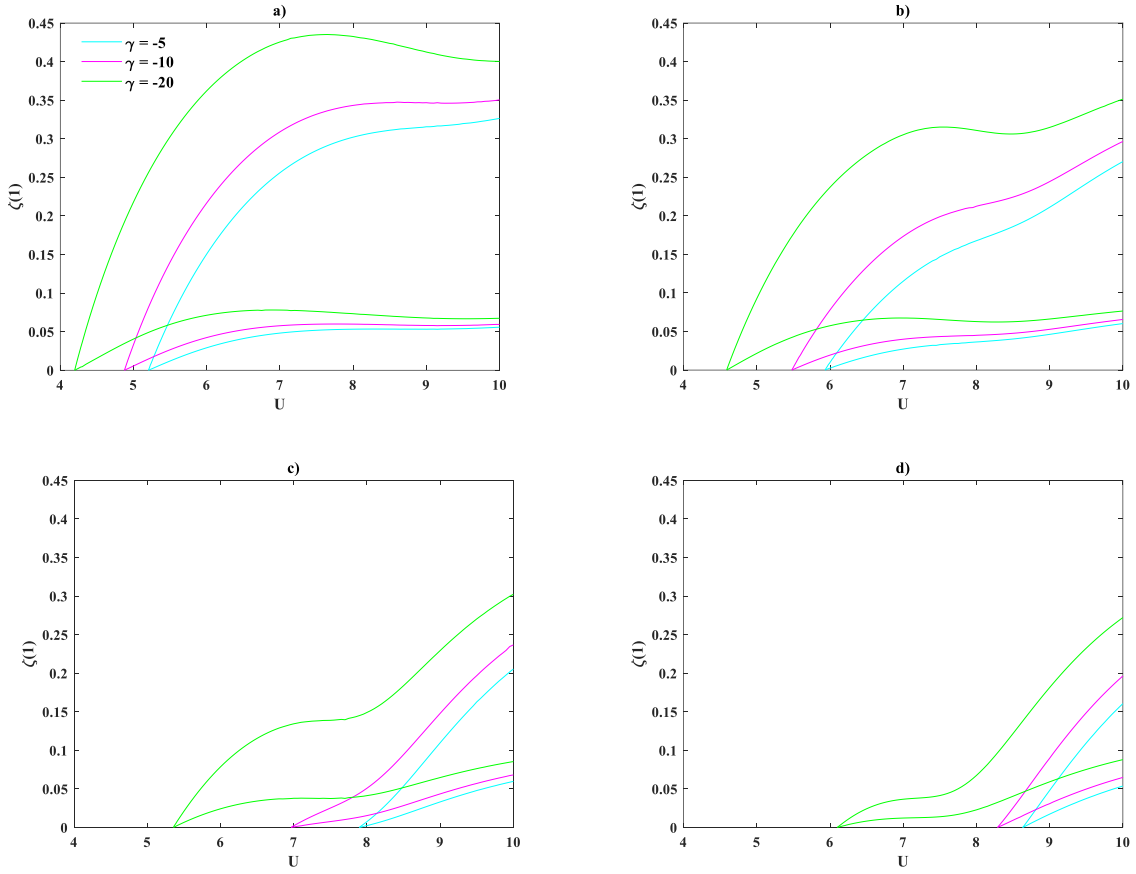

Figure 16: The tip axial displacement of pipe in the post-flutter region corresponding to Figure 14; a) $\beta = 0.17$, b) $\beta = 0.25$, c) a) $\beta = 0.37$, d) $\beta = 0.45$.

The general behavior of system with $\gamma = -30$ when $\beta = 0.17, 0.25, 0.37,$ and 0.45 are demonstrated in Figures 17-19 for the tip rotation angle, tip axial, and transverse displacements, respectively. For the system with $\gamma = -30$, the unstable and stable critical flow velocities, which

are related to the subcritical buckling, occur at $U_{sub}^{low} = 3.0726$ and U_{sub}^{high} =4.0618, respectively. On the other hand, the critical flow velocities related to the flutter instability of $\beta = 0.17, 0.25, 0.37,$ and 0.45 are $U^f = 3.4732, 3.690, 4.0836,$ and 4.3853, respectively. Comparing U_{sub}^{high} and U^f shows that for $\beta = 0.17$ and 0.25, U^f is smaller than U_{sub}^{high} which means that for $U_{sub}^{low} < U < U^f$, the system has three stable positions including two symmetric stable positions due to the subcritical buckling, along with its undeformed configuration, and for $U^f < U < U_{sub}^{high}$, the system may undergo post-buckling or post-flutter (see Figures 17-19 a-b). Since $U^f > U_{sub}^{high}$ for $\beta = 0.37$ and 0.45, a similar scenario to that described for the system with $\beta = 0.17$ and $\gamma = -20$ takes place for these cases. The described scenario for the system with $\gamma = -30$ when $\beta = 0.17$ or 0.25 can occur for $\beta = 0.37$ and 0.45 when the gravity parameter becomes small enough in which $U^f < U_{sub}^{high}$ (see Figure 7).

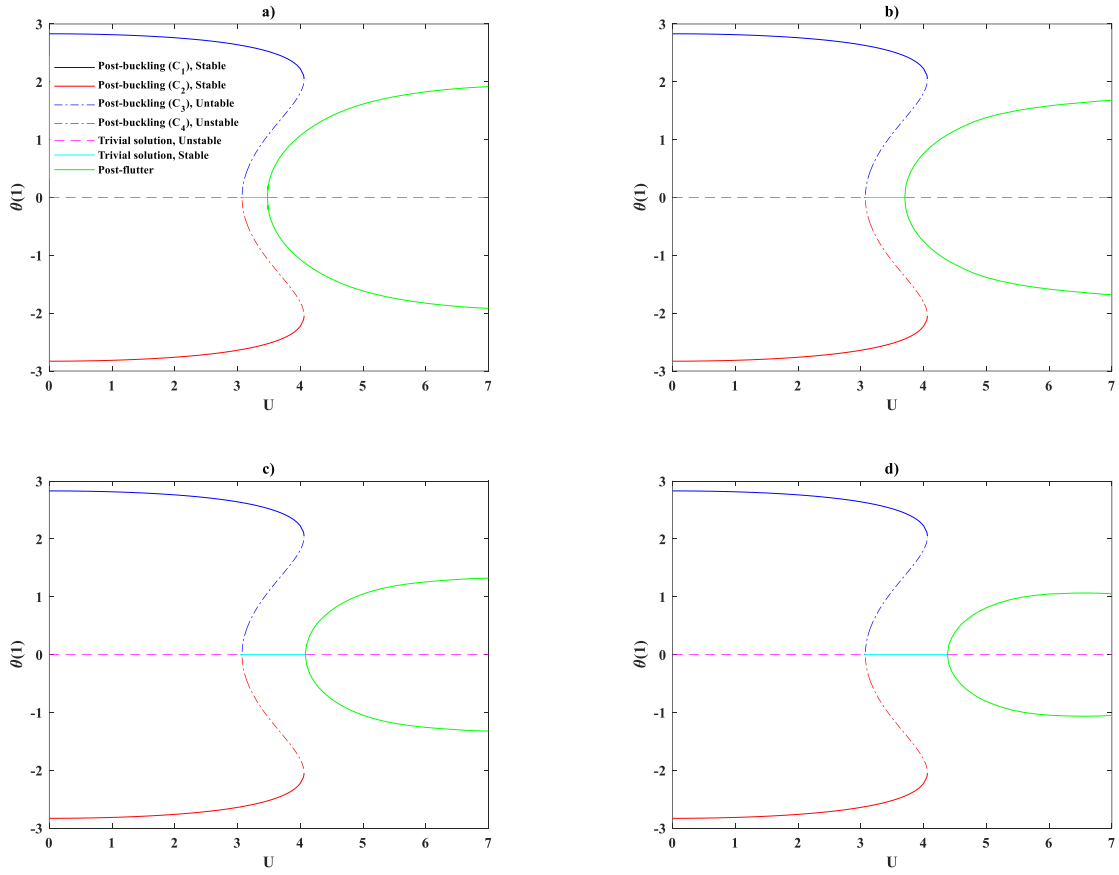

Figure 17: The tip rotation of pipe when $\gamma = -30$; a) $\beta = 0.17$, b) $\beta = 0.25$, c) $\beta = 0.37$, c) $\beta = 0.45$.

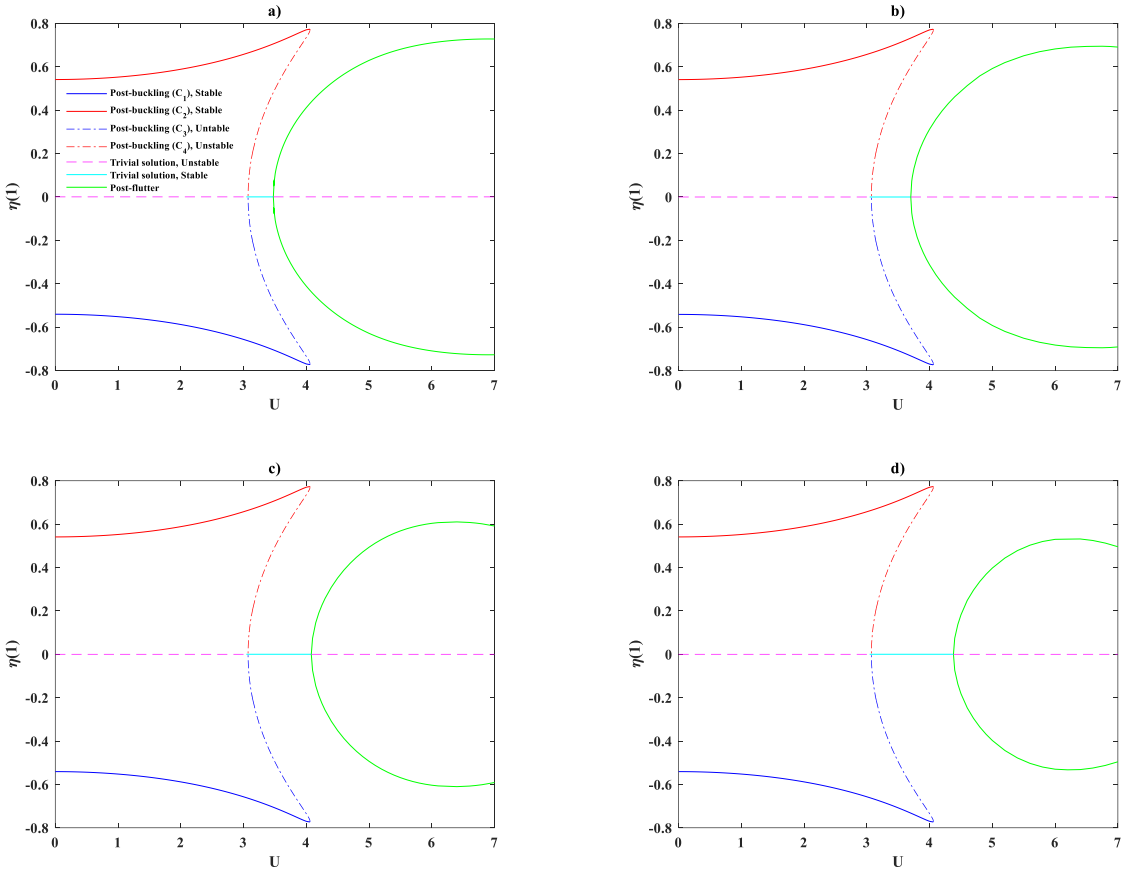

Figure 18: The tip transverse displacement of pipe of pipe corresponding to Figure 17; a) $\beta = 0.17$, b) $\beta = 0.25$, c) $\beta = 0.37$, c) $\beta = 0.45$.

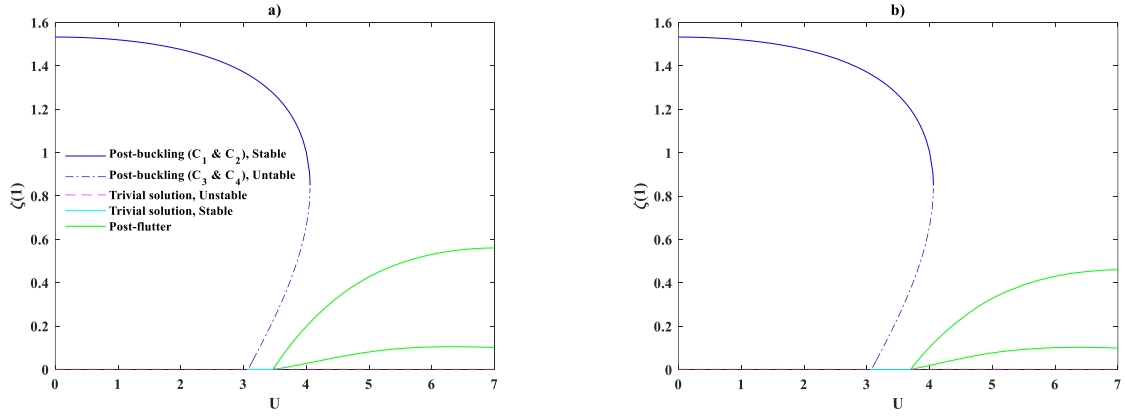

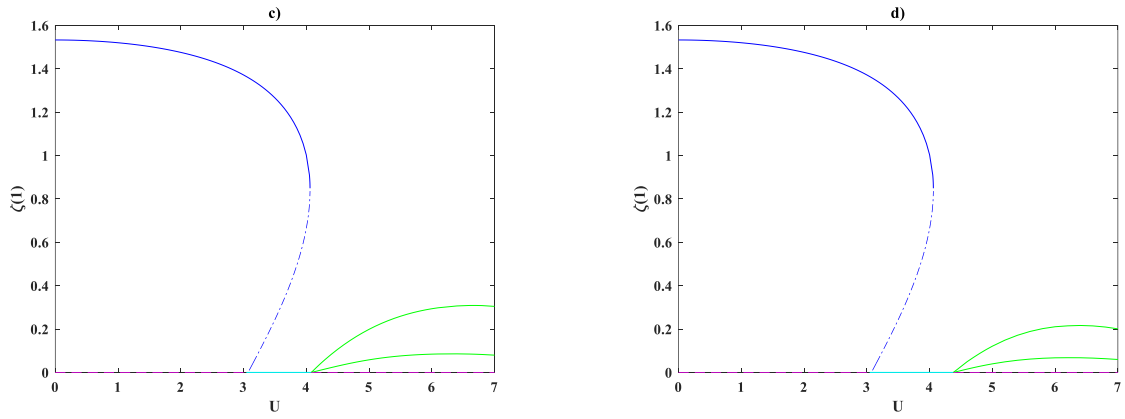

Figure 19: The tip axial displacement of pipe of pipe corresponding to Figure 17; a) $\beta = 0.17$, b) $\beta = 0.25$, c) $\beta = 0.37$, c) $\beta = 0.45$.

The general deformed shapes of system with $\gamma = -30$ and $\beta = 0.17$ for $U = 3, 3.25, 4$, and 4.25 are exhibited in Figure 20. The plotted results indicate that the system has two symmetric stable positions when $U = 3$, but it finds three stable positions when $U = 3.25$. Additionally, the system may undergo post-buckling or post-flutter when $U = 4$, but it only undergoes post-flutter when $U = 4.25$. The dynamic responses of system for $U = 3.25$ and 4 under different initial conditions with positive values are plotted in Figure 21. The depicted results in Figure 21a related to Figure 20b indicate that the system settles down at both the post-buckled position and undeformed configuration depending on the initial conditions. Besides, the results plotted in Figure 21b corresponding to Figure 20c illustrate that both the post-buckling or post-flutter scenarios can occur for the system depending on the initial conditions. However, both the plots in the figure show that the initial conditions do not affect the amplitude of post-buckled position and also the amplitude and frequency of post-flutter response. The responses of system with $\beta = 0.17$ and 0.45 when $U = 4.25$ are also shown in Figure 22. In the case of $\beta = 0.17$ corresponding to Figure 20c, the only response of system is post-flutter and in the case of $\beta = 0.45$ (see Figure 17a) the only response of system is its undeformed configuration. The plots in Figure 22 demonstrate that the final steady-state response is independent of the initial conditions for both cases.

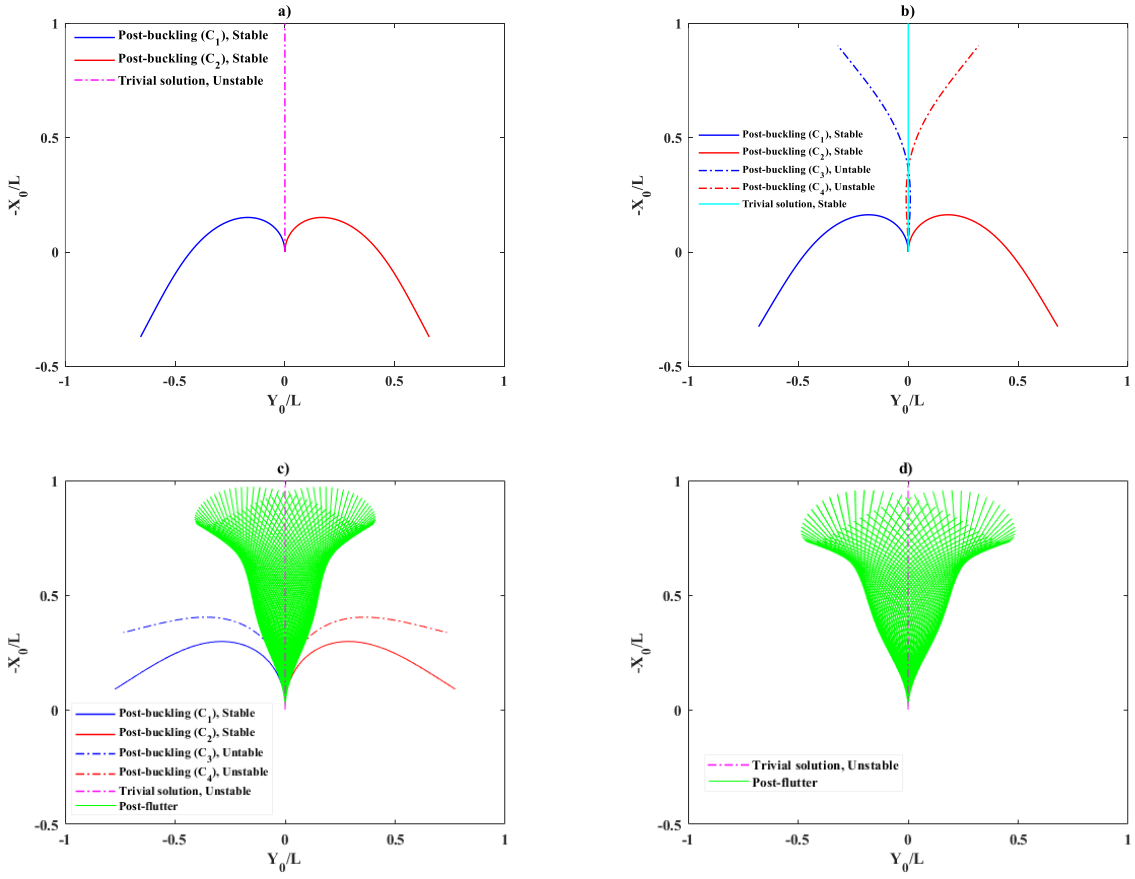

Figure 20: Shapes of the pipe when $\beta = 0.17$, $\gamma = -30$; a) $U = 3$, b) $U = 3.25$, c) $U = 4$, d) $U = 4.25$.

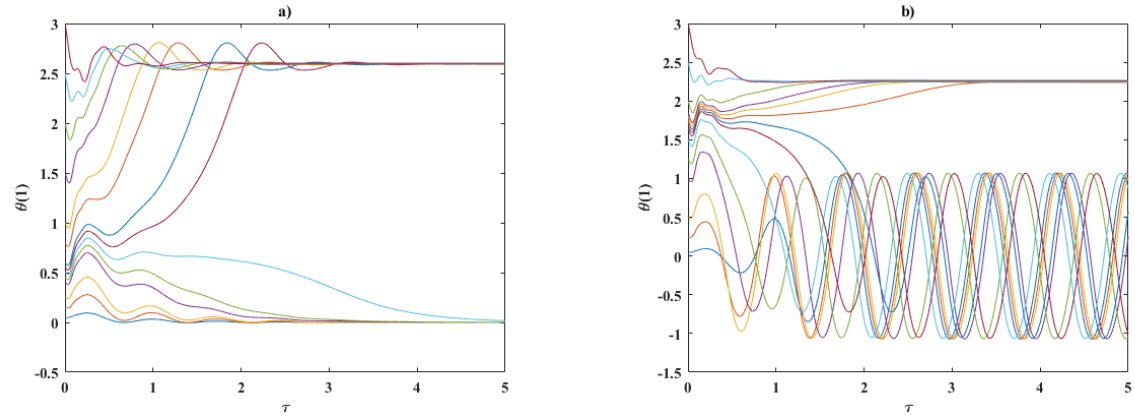

Figure 21: Time trace for the tip rotation of pipe under different initial conditions when $\beta = 0.17$, $\gamma = -30$; a) $U = 3.25$, b) $U = 4$.

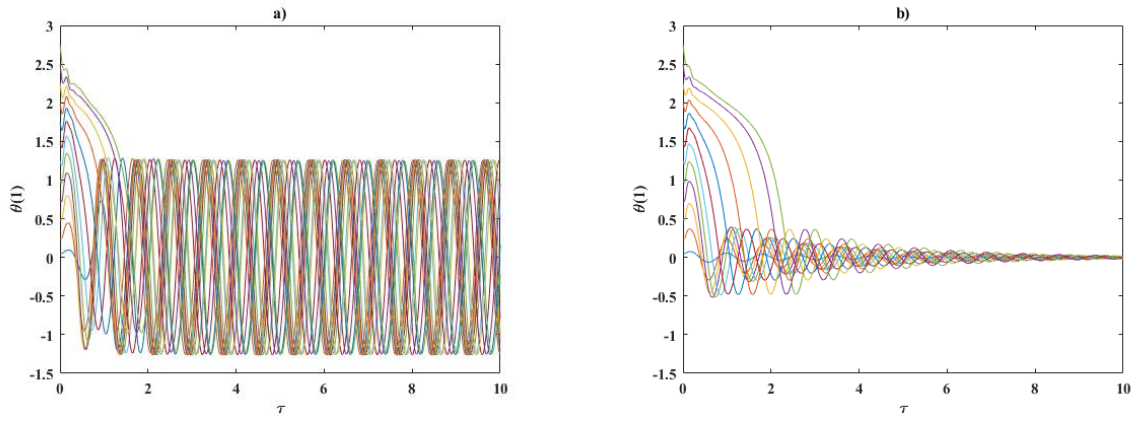

Figure 22: Time trace for the tip rotation of pipe under different initial conditions when $\gamma = -30$, and $U = 4.25$; a) $\beta = 0.17$, b) $\beta = 0.45$.

5. Conclusion

In the current study, the geometrically exact static responses and their stability characteristics for the standing cantilevered pipe conveying fluid are examined when the gravity parameter is in the range of $-100 \leq \gamma \leq 0$. The geometrically exact dynamic behavior, as well as the generic behavior of system, is also examined for $-30 \leq \gamma$, different values of the mass ratio $\beta = 0.17, 0.25, 37$, and 0.45 when the flow velocity is in the range of $0 \leq U \leq 10$. Additionally, the geometrically exact quaternion-based model utilized for the dynamic analysis is verified by using the reported results in Ref. [50] which were obtained by the geometrically exact rotation-based model.

The generic behavior of standing cantilevered pipe conveying fluid is strongly dependent on the gravity parameter, unlike the hanging one. It is due to the fact that a standing pipe with zero flow velocity may lose its stability and buckle due to its weight and it may undergo extremely large amplitude. Therefore, its undeformed configuration may not be stable, unlike the hanging one. The standing cantilevered pipe conveying fluid undergoes supercritical and subcritical bucklings when $-14 \leq \gamma < -7.83$ and $\gamma < -14$, respectively. As well, the unstable critical flow velocity related to the subcritical buckling becomes zero at $\gamma = -55.9$ and this critical flow velocity disappears for $\gamma > -55.9$. In the case of supercritical buckling, the stable post-buckled branches become zero at a supercritical flow velocity when the flow velocity is increased, but these stable branches do not meet zero in the case of subcritical buckling. Moreover, in the subcritical buckling domain, the impact of increasing the flow velocity on the deformation of system diminishes when the gravity parameter is lessened.

The system undergoes flutter instability by a supercritical Hopf bifurcation in which the mass ratio, together with the gravity parameter plays a significant role in the critical flow velocity in which the flutter occurs, as well as in the motion characteristics of self-excited periodic oscillations in the post-flutter region (see Figure 14). The stability of undeformed configuration prior to flutter is dependent on the gravity parameter. In the case of $\gamma \geq -7.83$, the undeformed configuration is

stable before flutter. In the supercritical/subcritical buckling domain, it is unstable and becomes stable at the supercritical/unstable subcritical flow velocity and again loses its stability by flutter. In view of the described supercritical/subcritical buckling and supercritical Hopf bifurcation, four different scenarios come to pass when the flow velocity is increased. In the first scenario, the undeformed configuration of system is stable and becomes unstable via a flutter instability (see Figure 8a), similar to the hanging one. In the second scenario, the undeformed configuration of system is unstable, but it becomes stable via a supercritical buckling and remains stable previous to losing its stability via a flutter (see Figure 8b). In the third scenario, the system undergoes subcritical buckling and the undeformed configuration becomes stable at the lower subcritical flow velocity and then loses its stability via a flutter (Figures 8c and 17c-d). A main difference between this scenario with the previous one is the undeformed configuration and the symmetric stable positions due to the subcritical buckling are the stable positions of system when the flow velocity is between the lower and higher subcritical flow velocities. The fourth scenario is similar to the third one but with a major difference. In this scenario, the critical flow velocity in which the flutter instability takes place is between the lower and higher subcritical flow velocities (Figures 17a-b). In other words, the system undergoes post-buckling or post-flutter for some flow velocities. The dynamic analyses with a focus on the role of initial conditions indicate that different responses predicted for a specific case can be achieved when appropriate initial conditions are applied.

Appendix A

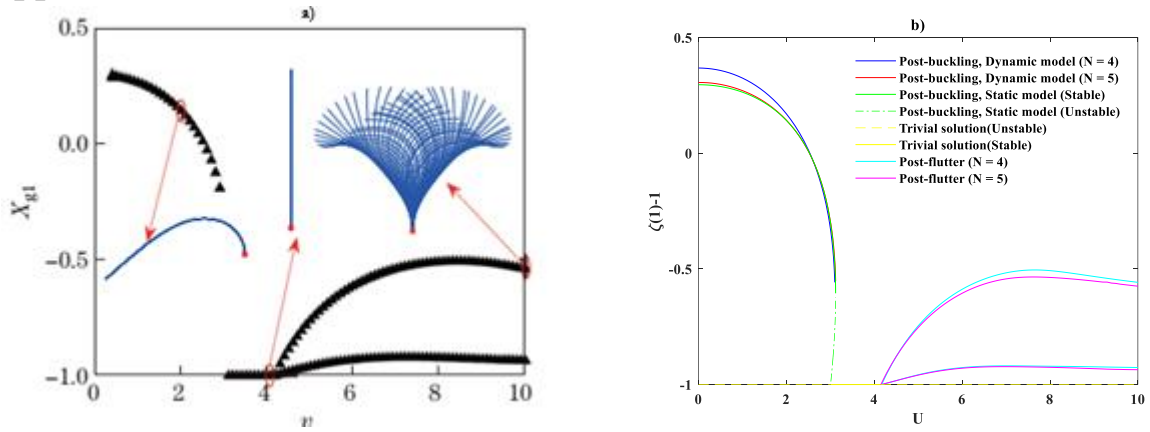

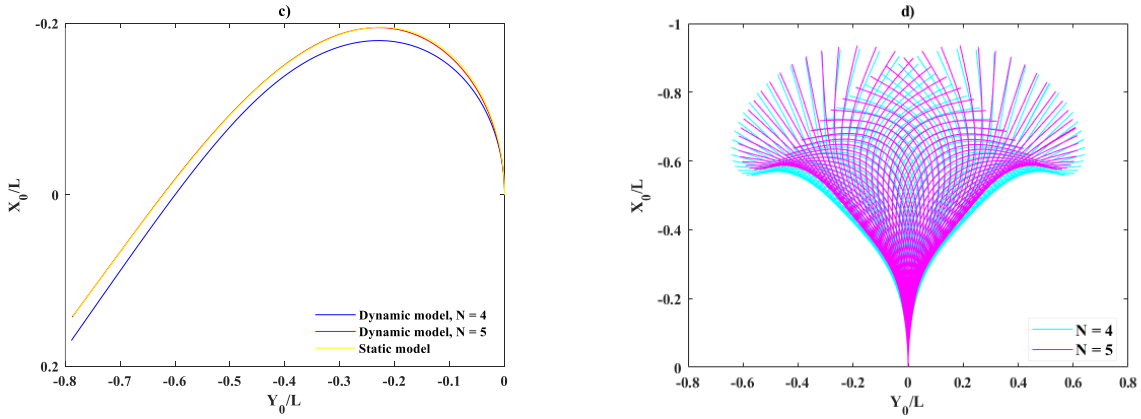

Figure A1: Comparison studies for the tip axial displacements and shapes of pipe when $\beta = 0.142$, $\gamma = -18.9$, and $\alpha = 0.005$ a) Chen et al. [50] via the geometrically exact rotation-based model with $N = 4$, b, c, and d) present study using the geometrically exact quaternion-based model with $N = 4$ & 5.

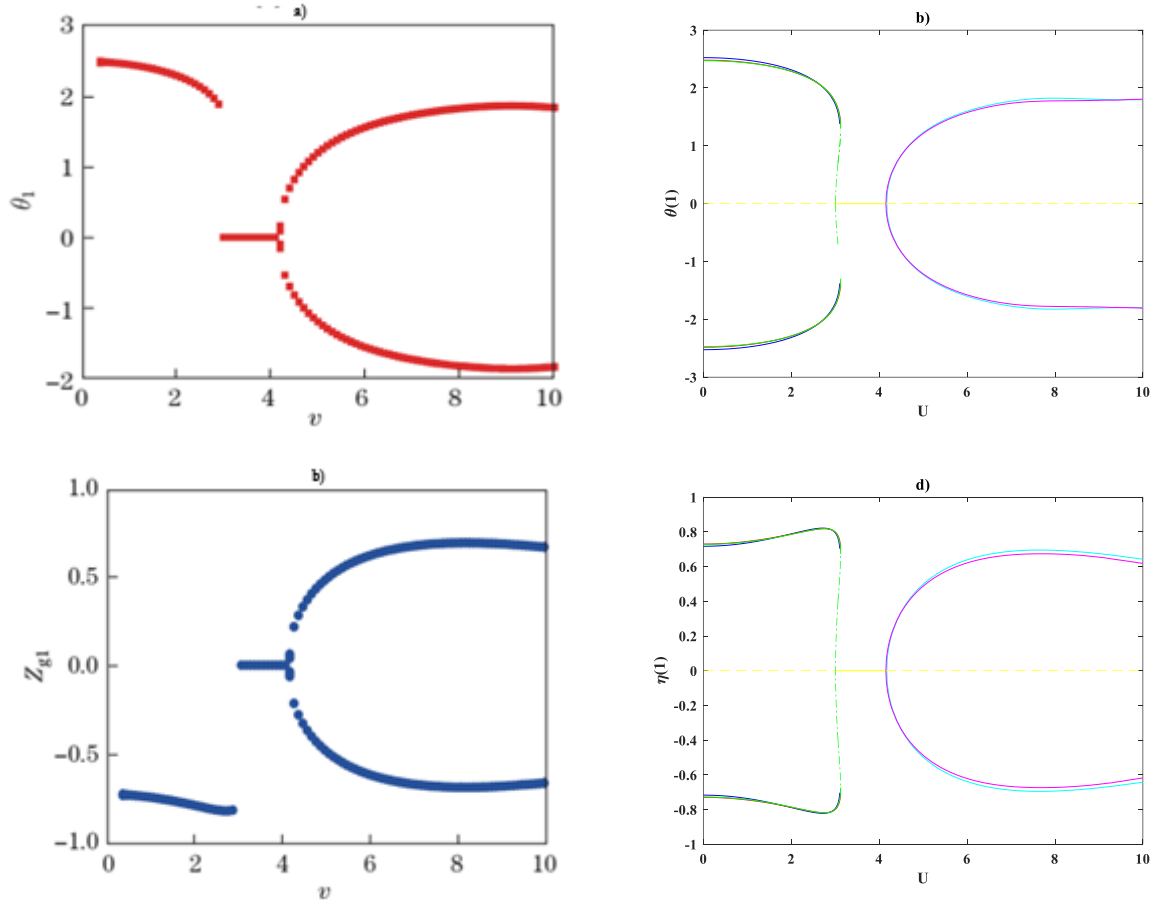

Figure A2: Comparison studies for the tip rotations and tip transverse displacements of pipe corresponding to Figure A1a-b; a & c) Chen et al. [50], b & d) present study.

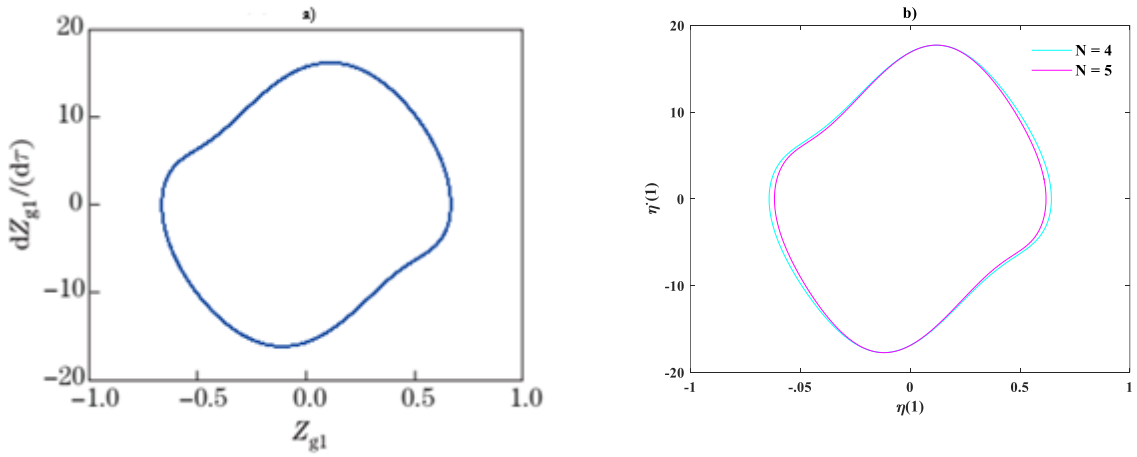

Figure A3: Comparison studies for the phase plane of pipe corresponding to Figure A1a & d; a) Chen et al. [50], b) present study.

References

[1] R. A. Ibrahim, "Overview of mechanics of pipes conveying fluids—Part I: Fundamental studies," *Journal of Pressure Vessel Technology, Transactions of the ASME,* vol. 132, no. 3, pp. 0340011 - 03400132, 2010.

[2] R. A. Ibrahim, "Mechanics of pipes conveying fluids—part II: applications and fluidelastic problems," *Journal of Pressure Vessel Technology, Transactions of the ASME,* vol. 133, no. 2, p. 024001, 2011.

[3] M. P. Païdoussis, *Fluid-structure interactions: slender structures and axial flow*, Second ed. Elsevier, 2014.

[4] M. P. Païdoussis, "Pipes conveying fluid: a fertile dynamics problem," *Journal of Fluids and Structures,* vol. 114, p. 103664, 2022.

[5] H. Ding and J. C. Ji, "Vibration control of fluid-conveying pipes: a state-of-the-art review," *Applied Mathematics and Mechanics,* vol. 44, no. 9, pp. 1423-1456, 2023.

[6] Q. Jin and Y. Ren, "Review on mechanics of fluid-conveying nanotubes," *International Journal of Engineering Science,* vol. 195, p. 104007, 2024.

[7] P. J. Holmes, "Pipes supported at both ends cannot flutter," *Journal of Applied Mechanics,* vol. 45, no. 3, pp. 619–622, 1978.

[8] M. Yoshizawa, H. Nao, E. Hasegawa, and Y. Tsujioka, "Buckling and postbuckling behavior of a flexible pipe conveying fluid," *Bulletin of JSME,* vol. 28, no. 240, pp. 1218-1225, 1985.

[9] M. Nikolić and M. Rajković, "Bifurcations in nonlinear models of fluid-conveying pipes supported at both ends," *Journal of Fluids and Structures,* vol. 22, no. 2, pp. 173-195, 2006.

[10] Y. Modarres-Sadeghi and M. P. Païdoussis, "Nonlinear dynamics of extensible fluid-conveying pipes, supported at both ends," *Journal of Fluids and Structures,* vol. 25, no. 3, pp. 535-543, 2009.

[11] Y.-L. Zhang and L.-Q. Chen, "External and internal resonances of the pipe conveying fluid in the supercritical regime," *Journal of Sound and Vibration,* vol. 332, no. 9, pp. 2318-2337, 2013.

[12] J.-R. Yuan and H. Ding, "Three-dimensional dynamic model of the curved pipe based on the absolute nodal coordinate formulation," *Mechanical Systems and Signal Processing,* vol. 194, p. 110275, 2023.
[13] B. Zhu, X. Zhang, and T. Zhao, "Nonlinear planar and non-planar vibrations of viscoelastic fluid-conveying pipes with external and internal resonances," *Journal of Sound and Vibration,* vol. 548, p. 117558, 2023.
[14] Y. Guo, J.-a. Li, B. Zhu, and Y. Li, "Nonlinear dynamical model of hyperelastic pipes conveying fluid with finite deformation: roles of hyperelasticity and nonlinearity," *Nonlinear Dynamics,* pp. 1-18, 2023.
[15] M.-Y. Hao, H. Ding, X.-Y. Mao, and L.-Q. Chen, "Multi-harmonic resonance of pipes conveying fluid with pulsating flow," *Journal of Sound and Vibration,* vol. 569, p. 117990, 2024.
[16] Y. Tang, G. Wang, T. Yang, and Q. Ding, "Nonlinear dynamics of three-directional functional graded pipes conveying fluid with the integration of piezoelectric attachment and nonlinear energy sink," *Nonlinear Dynamics,* vol. 111, no. 3, pp. 2415-2442, 2023.
[17] F.-J. Bourrières, "Sur un phénomène d'oscillation auto-entretenue en mécanique des fluides réels," *Publications Scientifiques Et Techniques Du Ministère de L'air* vol. 147, 1939.
[18] T. B. Benjamin, "Dynamics of a system of articulated pipes conveying fluid-I. Theory," *Proceedings of the Royal Society of London. Series A. Mathematical and Physical Sciences,* vol. 261, no. 1307, pp. 457-486, 1961.
[19] T. B. Benjamin, "Dynamics of a system of articulated pipes conveying fluid. II. Experiments," *Proceedings of the Royal Society A: Mathematical, Physical and Engineering Sciences,* pp. 487-499, 1961.
[20] M. P. Païdoussis and R. W. Gregory, "Unstable oscillation of tubular cantilevers conveying fluid. I. theory," *Proceedings of the Royal Society of London,* vol. 293, no. 1435, pp. 512-527, 1966.
[21] R. W. Gregory and M. P. Paidoussis, "Unstable oscillation of tubular cantilevers conveying fluid II. Experiments," *Proceedings of the Royal Society of London. Series A. Mathematical and Physical Sciences,* vol. 293, no. 1435, pp. 528-542, 1966.
[22] A. K. Bajaj, P. R. t. Sethna, and T. S. Lundgren, "Hopf bifurcation phenomena in tubes carrying a fluid," *SIAM Journal on Applied Mathematics,* vol. 39, no. 2, pp. 213-230, 1980.
[23] A. K. Bajaj and P. R. Sethna, "Flow induced bifurcations to three-dimensional oscillatory motions in continuous tubes," *SIAM Journal on Applied Mathematics,* vol. 44, no. 2, pp. 270-286, 1984.
[24] C. Semler, G. X. Li, and M. Paıdoussis, "The non-linear equations of motion of pipes conveying fluid," *Journal of Sound and Vibration,* vol. 169, no. 5, pp. 577-599, 1994.
[25] M. Wadham-Gagnon, M. P. Paı, and C. Semler, "Dynamics of cantilevered pipes conveying fluid. Part 1: Nonlinear equations of three-dimensional motion," *Journal of fluids and structures,* vol. 23, no. 4, pp. 545-567, 2007.
[26] Y. Modarres-Sadeghi, M. P. Païdoussis, and C. Semler, "Three-dimensional oscillations of a cantilever pipe conveying fluid," *International Journal of Non-Linear Mechanics,* vol. 43, no. 1, pp. 18-25, 2008.
[27] M. H. Ghayesh, M. P. Païdoussis, and Y. Modarres-Sadeghi, "Three-dimensional dynamics of a fluid-conveying cantilevered pipe fitted with an additional spring-support and an end-mass," *Journal of Sound and Vibration,* vol. 330, no. 12, pp. 2869-2899, 2011.

[28] G. H. Chang and Y. Modarres-Sadeghi, "Flow-induced oscillations of a cantilevered pipe conveying fluid with base excitation," *Journal of Sound and Vibration,* vol. 333, no. 18, pp. 4265-4280, 2014.
[29] A. M. Dehrouyeh-Semnani, H. Zafari-Koloukhi, E. Dehdashti, and M. Nikkhah-Bahrami, "A parametric study on nonlinear flow-induced dynamics of a fluid-conveying cantilevered pipe in post-flutter region from macro to micro scale," *International Journal of Non-Linear Mechanics,* vol. 85, pp. 207-225, 2016.
[30] Y. Wang, L. Wang, Q. Ni, H. Dai, H. Yan, and Y. Luo, "Non-planar responses of cantilevered pipes conveying fluid with intermediate motion constraints," *Nonlinear Dynamics,* vol. 93, pp. 505-524, 2018.
[31] M. Kheiri, "Nonlinear dynamics of imperfectly-supported pipes conveying fluid," *Journal of Fluids and Structures,* vol. 93, p. 102850, 2020.
[32] K. Yamashita, N. Nishiyama, K. Katsura, and H. Yabuno, "Hopf-Hopf interactions in a spring-supported pipe conveying fluid," *Mechanical Systems and Signal Processing,* vol. 152, p. 107390, 2021.
[33] Y. Guo, B. Zhu, and Y. Li, "Flow-induced instability and bifurcation in cantilevered composite double-pipe systems," *Ocean Engineering,* vol. 258, p. 111825, 2022.
[34] K. Yamashita, K. Kitaura, N. Nishiyama, and H. Yabuno, "Non-planar motions due to nonlinear interactions between unstable oscillatory modes in a cantilevered pipe conveying fluid," *Mechanical Systems and Signal Processing,* vol. 178, p. 109183, 2022.
[35] M. Riazat and M. Kheiri, "Three-dimensional nonlinear dynamics of imperfectly supported pipes conveying fluid," *Journal of Fluids and Structures,* vol. 123, p. 104011, 2023.
[36] M. H. Ghayesh, M. P. Païdoussis, and M. Amabili, "Nonlinear dynamics of cantilevered extensible pipes conveying fluid," *Journal of Sound and Vibration,* vol. 332, no. 24, pp. 6405-6418, 2013.
[37] J. Rivero-Rodriguez and M. Pérez-Saborid, "Numerical investigation of the influence of gravity on flutter of cantilevered pipes conveying fluid," *Journal of Fluids and Structures,* vol. 55, pp. 106-121, 2015.
[38] S. Tang and B. Sweetman, "A geometrically-exact momentum-based nonlinear theory for pipes conveying fluid," *Journal of Fluids and Structures,* vol. 100, p. 103190, 2021.
[39] W. Chen, H. Dai, Q. Jia, and L. Wang, "Geometrically exact equation of motion for large-amplitude oscillation of cantilevered pipe conveying fluid," *Nonlinear Dynamics,* vol. 98, pp. 2097-2114, 2019.
[40] H. Farokhi, M. Tavallaeinejad, and M. P. Païdoussis, "Geometrically exact dynamics of cantilevered pipes conveying fluid," *Journal of Fluids and Structures,* vol. 106, p. 103364, 2021.
[41] W. Chen, H. Dai, and L. Wang, "Three-dimensional dynamical model for cantilevered pipes conveying fluid under large deformation," *Journal of Fluids and Structures,* vol. 105, p. 103329, 2021.
[42] W. Chen, K. Zhou, L. Wang, and Z. Yin, "Geometrically exact model and dynamics of cantilevered curved pipe conveying fluid," *Journal of Sound and Vibration,* vol. 534, p. 117074, 2022.
[43] R. Cao, Z. Guo, W. Chen, H. Dai, and L. Wang, "Nonlinear dynamics of a circular curved cantilevered pipe conveying pulsating fluid based on the geometrically exact model," *Applied Mathematics and Mechanics,* vol. 45, no. 2, pp. 261-276, 2024.

[44] W. Chen, L. Wang, and Z. Peng, "A magnetic control method for large-deformation vibration of cantilevered pipe conveying fluid," *Nonlinear Dynamics,* vol. 105, pp. 1459-1481, 2021.
[45] A. M. Dehrouyeh-Semnani, "Nonlinear geometrically exact dynamics of fluid-conveying cantilevered hard magnetic soft pipe with uniform and nonuniform magnetizations," *Mechanical Systems and Signal Processing,* vol. 188, p. 110016, 2023.
[46] A. M. Dehrouyeh-Semnani, "A quaternion-based mathematical model for geometrically exact dynamic analysis of cantilevered pipe conveying fluid," *Nonlinear Dynamics, DOI: https://doi.org/10.1007/s11071-024-09609-5,* 2024.
[47] G. X. Li and M. P. Paidoussis, "Stability, double degeneracy and chaos in cantilevered pipes conveying fluid," *International Journal of Non-linear Mechanics,* vol. 29, no. 1, pp. 83-107, 1994.
[48] L. Wang and Q. Ni, "A note on the stability and chaotic motions of a restrained pipe conveying fluid," *Journal of sound and vibration,* vol. 296, no. 4-5, pp. 1079-1083, 2006.
[49] N. M. Bou-Rabee, L. A. Romero, and A. G. Salinger, "A multiparameter, numerical stability analysis of a standing cantilever conveying fluid," *SIAM journal on applied dynamical systems,* vol. 1, no. 2, pp. 190-214, 2002.
[50] W. Chen, Z. Hu, H. Dai, and L. Wang, "Extremely large-amplitude oscillation of soft pipes conveying fluid under gravity," *Applied Mathematics and Mechanics,* vol. 41, no. 9, pp. 1381-1400, 2020.
[51] B. D. Texier and S. Dorbolo, "Deformations of an elastic pipe submitted to gravity and internal fluid flow," *Journal of Fluids and Structures,* vol. 55, pp. 364-371, 2015.
[52] M. P. Paidoussis, "Dynamics of tubular cantilevers conveying fluid," *Journal of Mechanical Engineering Science,* vol. 12, no. 2, pp. 85-103, 1970.